Electronic Supplementary Material (ESI) for Reaction Chemistry & Engineering.

Supporting Information

Dynamic Experiments in Flow Accelerate Reaction Network Definition in a Complex Hydrogenation Using Catalytic Static Mixers

Stefano Martinuzzi,[ab] Markus Tranninger,[c] Peter Sagmeister,[ab] Martin Horn,[c]
Jason D. Williams,*[ab] C. Oliver Kappe*[ab]

[a]Center for Continuous Flow Synthesis and Processing (CCFLOW), Research Center Pharmaceutical Engineering GmbH (RCPE), Inffeldgasse 13, 8010 Graz, Austria
[b]Institute of Chemistry, University of Graz, NAWI Graz, Heinrichstrasse 28, 8010 Graz, Austria
[c]Institute of Automation and Control, Graz University of Technology, Inffeldgasse 21b, 8010 Graz, Austria

Contents

1. Continuous Flow Setup

1.1. General details

Solvents and chemicals were all obtained from commercial suppliers and were used without any further purification unless otherwise noted.

1.2. Detailed reaction setup

1.2.1. General

A photograph of the hydrogenation setup can be found below (Figure S1) and a schematic representation in manuscript Scheme 1. Each component is described in more detail in the subsequent sections. The continuous flow setup has been previously described.[1]

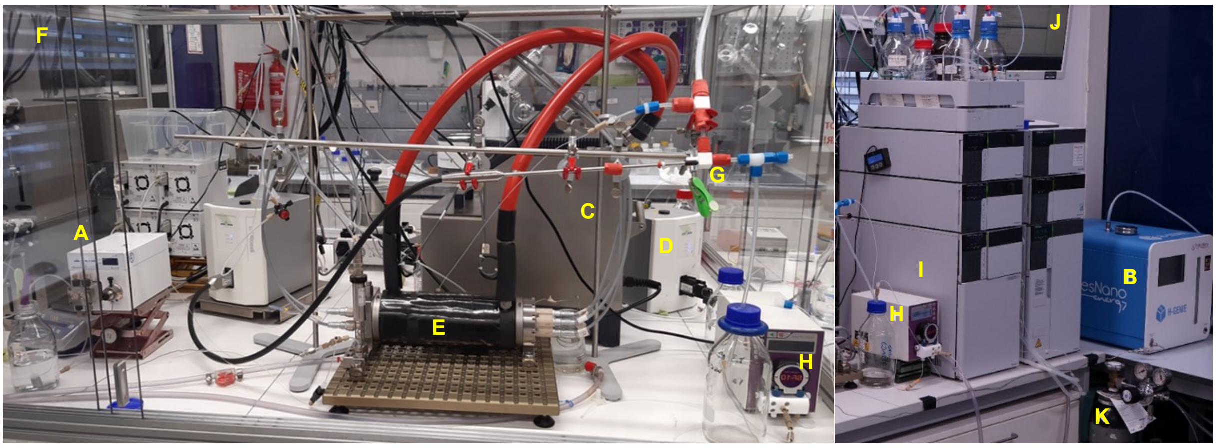

Figure S1. Labelled photograph of the hydrogenation setup; A: HPLC pump for liquid feed; B: H-Genie; C: thermostat; D: FT-IR; E: Miprowa Lab reactor; F: Enclosing cage; G: gas/liquid separator mounted on IR probe; H: peristaltic pump for UHPLC sampling; I: UHPLC; J: Computer for controlling and monitoring (not visible); K: N2-bottle leading to backpressure regulator (not visible on the figure).

1.2.2. Pump and liquid feed

The liquid feeds were delivered through perfluoro alkoxy alkane (PFA) tubing (inlet i.d. 1.6 mm, 1.2 mL; outlet: i.d. 0.8 mm, 1.8 mL) by a High-Performance Liquid Chromatography (HPLC) pump (Knauer, AZURA P 4.1S, Figure S2). The pump included an integrated pressure sensor. On the outlet of the pump a 30 bar BPR was placed just after the outlet of the pump to increase the operating pressure of the pump. The feed for the substrate was placed on a balance (Kern, KB 2400-2N) that allowed monitoring of the actual flow rate. The liquid feed then passed through PFA tubing (i.d. 0.8 mm, 1.8 mL) and another section of PFA tubing (i.d. 0.8 mm, 0.4 mL) to enter a PEEK Y-connector (i.d. 0.5 mm) for mixing with the hydrogen feed. All valves and connectors were supplied by IDEX.

Figure S2. Photograph of the HPLC pump used in the flow setup.

1.2.3. Hydrogen generator and mass flow controller

The hydrogen generator with an integrated mass flow controller (MFC) (ThalesNano Energy, H-Genie) was used for the introduction of hydrogen gas (Figure S3). The system was operated using HPLC grade water. The flow rate of H_2 was measured in NmL/min, where N represents measurement under standard conditions (i.e., $T_n = 0$ °C, $P_n = 1.01$ bar). The hydrogen was fed to the reactor via stainless-steel tubing (i.d. 0.8 mm, 2.6 mL), followed by a check valve and PFA tubing (i.d. 1.6 mm, 0.6 mL). The liquid and the hydrogen stream were combined in a Y-connector made from PEEK, which then passed through PFA tubing (i.d. 1.6 mm, 1.6 mL). The use of translucent tubing enabled observation of the slug flow regime within this section of the flow setup (Figure S4). The gas-liquid flow then entered the Modular Micro Reaction System (Ehrfeld, MMRS) via a 1/8" input connector (0711 2 0124 F, Hastelloy C-276) and a coaxial heat exchanger (0309-4-0004-F, Hastelloy C-276).

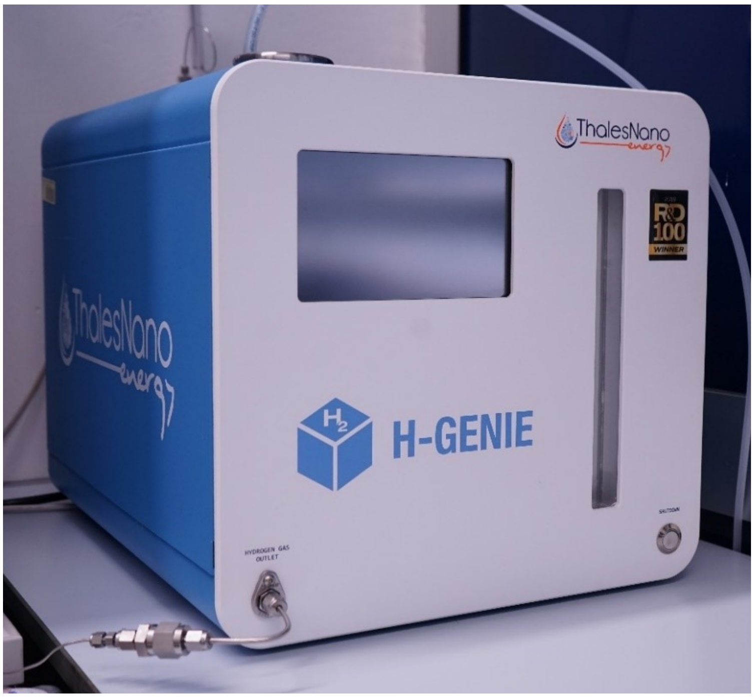

Figure S3. Photograph of the hydrogen generator.

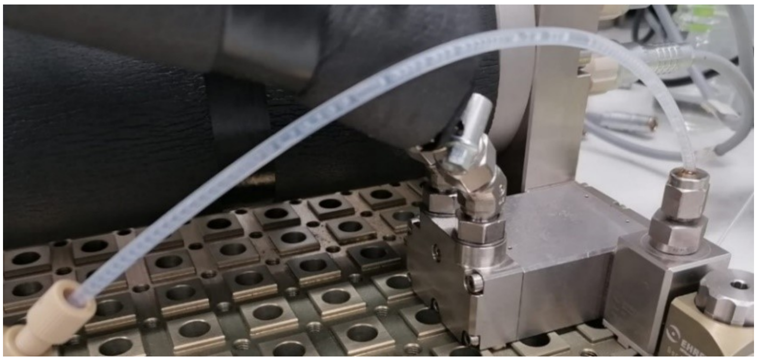

Figure S4. Process medium entering the reactor in slug flow regime.

1.2.4. Reactor

The hydrogenation reaction was performed in a Miprowa Lab reactor (Ehrfeld, 0224-2-2004-F, Hastelloy C-276) (Figure S5). This reactor contains reaction channels with a rectangular cross-section (1.5 mm × 12 mm × 300 mm). The flange (Figure S6) was used to reduce the number of active channels from 8 to 4. Only the first channel was filled with two catalytic static mixers (Precision Catalysts, Australia) of 150 mm length each (Figure S7) and used. Its outlet was directly connected to the cooling trap. The original exit of the reactor was blanked off and the other three channels were therefore not used. A previous study suggested that within the reactor the flow regime changed from slug flow to stratified flow, with the liquid phase adhering to the catalyst.[2]

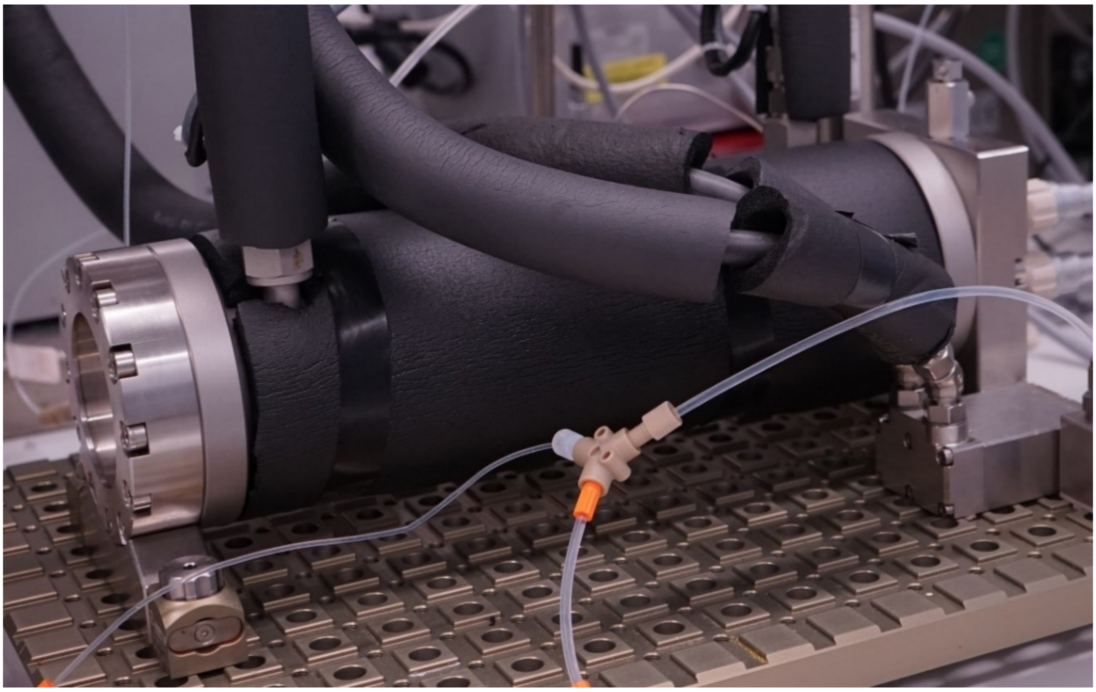

Figure S5. Photograph of the Miprowa Lab reactor and MMRS.

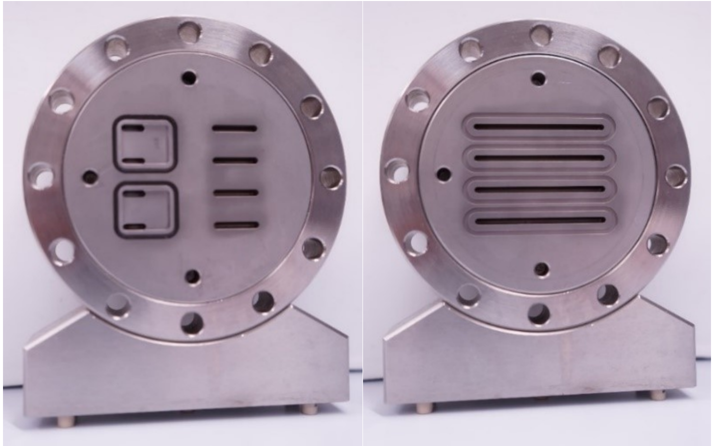

Figure S6. Photograph of the Flange in 4 (left) and 8 (right) channel orientation. *Note:* the *4-channel setup was used for all experiments discussed here.*

1.2.5. Catalytic Static Mixers

The catalytic static mixers (CSMs) were manufactured from 316L stainless steel powder by selective laser melting, according to a design by CSIRO. The 3D-printed static mixers were coated with Pd/Al_2O_3, Pt/Al_2O_3 and Ru/Al_2O_3 by Precision Catalysts via a slurry coating technique

A single test with an electroplated Pt CSM was carried out, but this was proved to be completely inactive and no further tests were carried out with this type of CSM. During the investigation, the following order of use of catalysts was used: Pd, Pt, Ru, Pt, Pd and therefore the same CSM was used for different runs at different times. Before and after each use the CSMs were weighed to check for changes in weight due to leaching. The reactor volume was calculated as 2.7 mL for each of the empty sections (one channel has 2 sections), or 1.7 mL for a section containing a static mixer. The dead volume after the reactor and before the FT-IR probe, consisting of a metal cooling coil (i.d. 0.8 mm) and PFA tubing (i.d. 0.8 mm) had a volume of 2.8 mL.

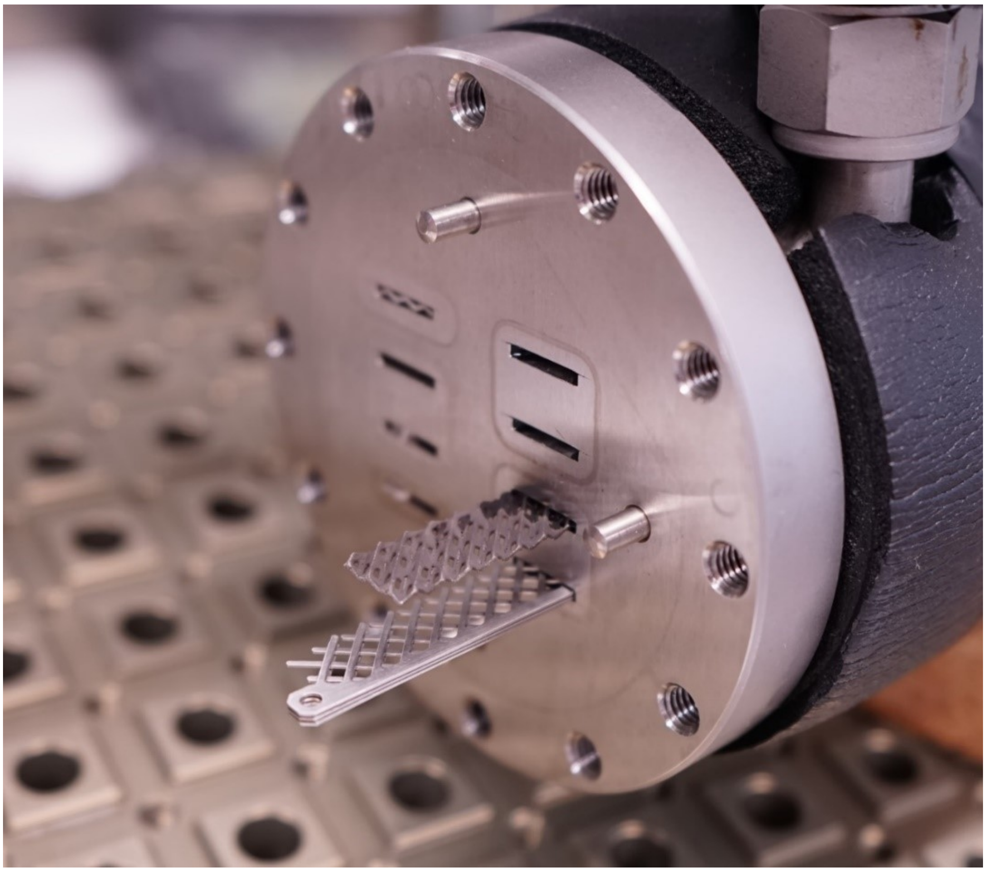

Figure S7. Photograph of the opened Miprowa Lab reactor, showing a standard static mixing element (bottom) and a CSM (top).

1.2.6. Temperature and pressure control

The temperature of the reactor and heat exchanger was adjusted using a thermostat (Huber, CC-304, Figure S8) and was monitored at two points for the process stream: 1) process medium input to reactor, 2) process medium output from reactor, and two points for the thermal fluid stream as well: 1) thermostat bath temperature, 2) thermal fluid output from the reactor. Due to alternating gas/liquid slugs, the temperature signal from the process medium was prone to oscillation, depending on the ratio and flow rates of the liquid and gas streams.

After the Miprowa Lab reactor, the reaction stream passed through a pressure sensor module (0518-1-60x4-F, Hastelloy C-276), a 1/16" output connector (0711 2 0124 F, Hastelloy C-276) and a stainless-steel coil (i.d. 0.8 mm, 1 mL), which was submerged in an actively-cooled water bath at ambient temperature, to cool the reaction output.

The pressure inside the system was controlled by a membrane-based back pressure regulator (Equilibar, Zero Flow BPR), regulated by a pressure controller (Bronkhorst, EL-PRESS) with attached PFA tubing (i.d. 1.6 mm, 0.8 mL in total) as in- and outlet. Unless otherwise stated, experiments were performed with the BPR set to 20 bar. At ambient pressure, after passing through PFA tubing (i.d. 0.8 mm, 2 mL) the excess hydrogen was separated by a custom-made gas-liquid separator, mounted on an inline Fourier Transform Infrared Spectroscopy (FT-IR) probe also containing an inlet tubing for online Ultra High-Performance Liquid Chromatography (UHPLC) sampling.

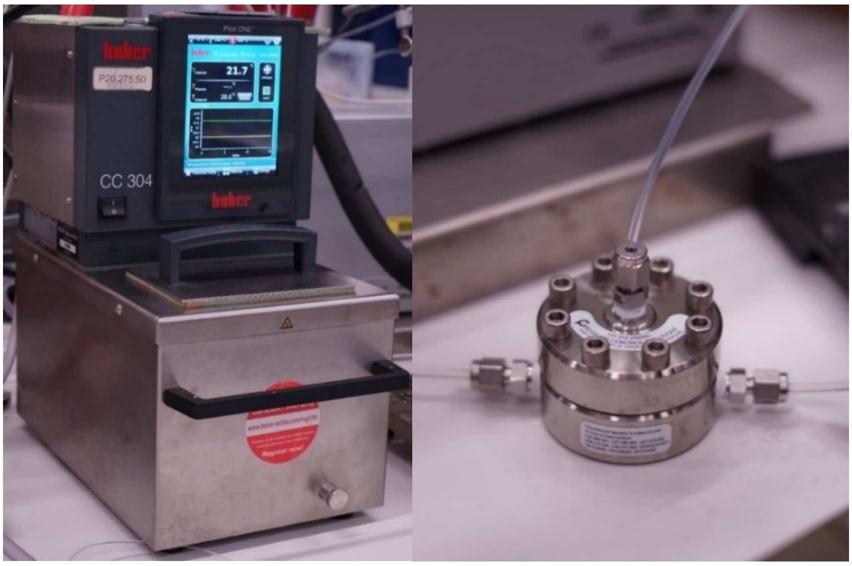

Figure S8. Photographs of the Huber CC-304 thermostat (left) and Equilibar BPR (right).

2. Determination of products and impurities

2.1. Offline analytical equipment

2.1.1. GC-FID

GC-FID analysis was performed on a Shimadzu GC FID 230 with a flame ionization detector, using an RTX-5MS column (30 m × 0.25 mm ID × 0.25 µm) and helium as carrier gas (40 cm/sec linear velocity). The injector temperature was set to 280 °C. After 1 min at 50 °C, the temperature was increased by 25 °C/min to 300 °C and kept constant at 300 °C for 4 min. The detector gases used for flame ionization were hydrogen and synthetic air (5.0 quality).

2.1.2. GC-MS

GC-MS was performed with a Shimadzu GCMS-QP2010 SE, using a Rtx-5MS column (30 m × 0.25 mm × 0.25 µm) and helium as carrier gas with a linear velocity of 40 cm/sec. The injector temperature was set to 280 °C. After 1 min at 50 °C, the oven temperature was increased by 25 °C/min to 300 °C and then kept at 300 °C for 3 min. The mass detector was a quadrupole with pre-rods and electron impact ionization. The following settings were used in the detector: ion source temperature 200 °C, interface temperature 310 °C, solvent cut time 2 min 30 sec, acquisition mode scan, mass range m/z = 50 till m/z = 400.

2.2. Identification of commercially available species

Some species formed could be identified thanks to their commercial availability. These species with their GC-FID retention times are listed below.

Species	Name	CAS	MW	Compound number	GC-FID Retention time
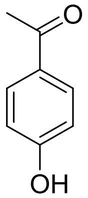	4-Hydroxyphenylethanone	99-93-4	136.15	1	6.85 min
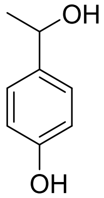	4-(1-Hydroxyethyl)-phenol	2380-91-8	138.16	2	7.24 min

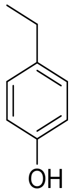	4-Ethylphenol	123-07-9	122.16	3	5.63 min
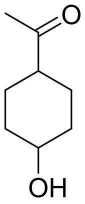	1-(4-Hydroxycyclohexyl) -ethanone	15580-01-5	142.20	4	6.24, 6.29 min
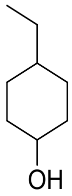	4-Ethylcyclohexanol	4534-74-1	128.21	6	4.94 min (two overlapping peaks)
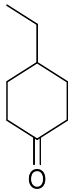	4-Ethylcyclohexanone	5441-51-0	126.20	-	5.06 min
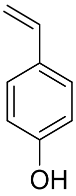	4-Hydroxystyrene	2628-17-3	120.15	9	5.95 min
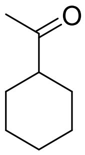	1-Cyclohexylethanone	823-76-7	126.20	-	4.80 min

Some of these species could be seen on the chromatograms only at very low level and therefore they were not considered during reaction monitoring.

2.3. Confirmation of identity of commercially unavailable species

The species which were not available had to be synthesized from available compounds. In the following sections the different synthetic procedures used are listed.

2.3.1. 1-Hydroxyethyl-cyclohexan-4-ol (7)

The synthesis of 1-hydroxyethyl-cyclohexan-4-ol (**7**) was performed using the procedure described below.

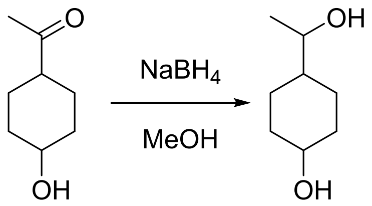

4 **7**

1-(4-Hydroxycyclohexyl)-ethanone (48.4 mg, BLDpharm, BD00764707, 95%) was added to a round bottom flask and dissolved in methanol (1 mL, VWR, 98.5%). Upon dissolution, a solution of NaBH4 (29.4 mg, Sigma Aldrich, 100%) in 2.5 mL of methanol was added at room temperature with stirring and left to react for 225 min. Full GC conversion was achieved and the product confirmed the identity of this species in the chromatogram. Both starting material and product are present as two diastereomer peaks in the GC-FID chromatogram: For the starting materials the retention times were 6.24 and 6.29 min, for the products 6.33 and 6.36 min.

2.3.2. 1-Hydroxyethyl-cyclohexane (8)

The synthesis of 1-hydroxyethyl-cyclohexane was performed using the procedure described below.

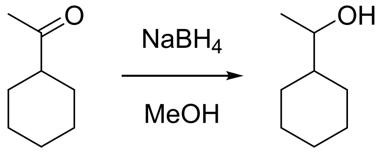

8

Cyclohexyl-methyl ketone (536.2 mg, Fisher Scientific, 95%) was added to a round bottom flask and dissolved in methanol (30 mL, VWR, 98.5%). Upon dissolution, a solution of $NaBH_4$ (606.2 mg, 3.77 eq., Sigma Aldrich, 100%) in 10 mL of methanol was added at room temperature under stirring and left to react for 250 min. 27% GC conversion was achieved and the product confirmed the identity of this species in the chromatogram, even though it was not isolated due to the low amount of product form. The starting material and the product had GC-FID retention times of 4.78 and 4.88 min respectively.

2.3.3. 4-(1-Hydroxyethyl)-cyclohexanone (5)

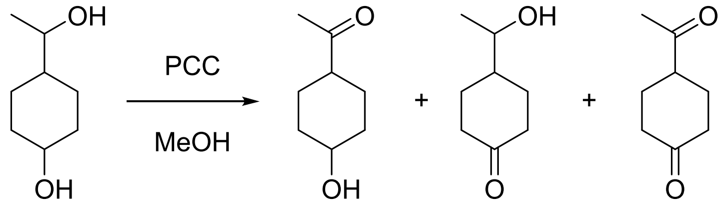

7 **4** **5**

1-Hydroxyethyl-cyclohexan-4-ol (1 mL of EtOAc solution, synthesized in 2.3.1) was added to a round bottom flask. Pyridinium chlorochromate (PCC, 5.8 mg, Sigma Aldrich, 98%) was added at room temperature under stirring. The solution was left to stir for 360 min. The reaction was followed by GC-FID (dilution of 50 µL of the mixture with 1 mL of diethyl ether and filtration to remove solids). The oxidation of 1-hydroxyethyl-cyclohexan-4-ol **7** led to the formation of 1-(4-hydroxycyclohexyl)-ethanone (starting material for the production of the former) and 4-(1-hydroxyethyl)-cyclohexanone, following the reaction in figure. The retention time of 4-(1-hydroxyethyl)-cyclohexanone was equal to 6.5 min.

2.3.1. Example GC-FID Chromatogram

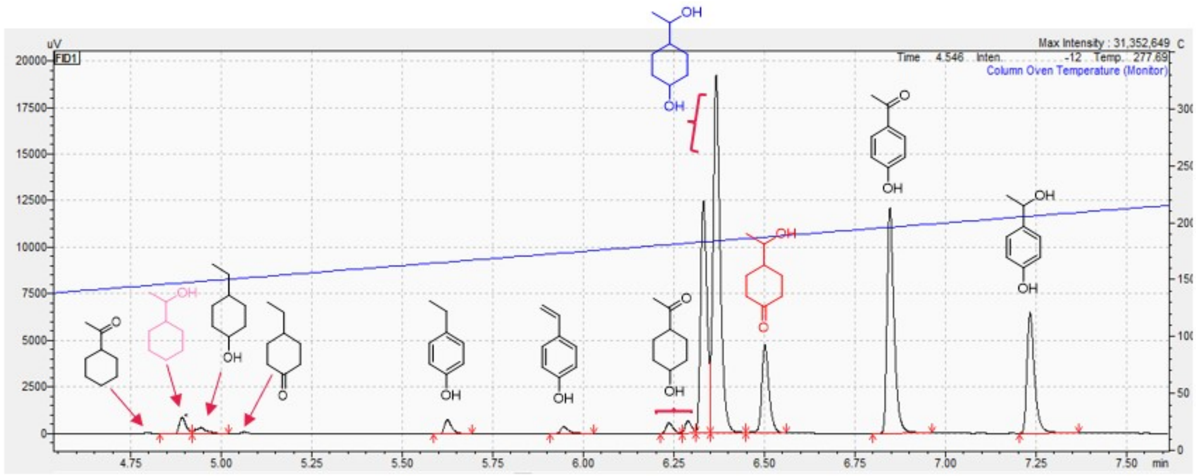

Figure S9. Example GC-FID chromatogram, showing the product distribution of a Pt/Al_2O_3-catalyzed reaction.

3. Process Analytical Technology

3.1. Inline FT-IR Spectroscopy

3.1.1. General

FT-IR measurements were made using a Mettler Toledo ReactIR 15 instrument, equipped with an AgX 9.5 mm fiber and a DiComp (diamond composite) probe. Sampling time was set to 15 s with a measured wavenumber range from 3400 to 800 cm^{-1} using the maximum resolution of 4 cm^{-1}. Prior to starting the experiments, it was ensured that the MCT (mercury cadmium telluride) detector was cooled with liquid nitrogen, so that the signal to noise ratio was above 15000 and the peak height was between 18000 and 24000 counts.

For inline monitoring of the process stream, the FT-IR probe was implemented directly after the atmospheric gas-liquid separator (polytetrafluoroethylene T-connector, Bola, 10.5 mm bore). The biphasic gas-liquid stream was introduced at the side connection, excess hydrogen was allowed to escape through the upper tubing (leading to an extractor). The liquid stream was allowed to flow downwards into a second PTFE T-connector (Bola, 6.5 mm bore) mounted in a tilted horizontal position. The FT-IR probe was inserted at the downward facing end (left in **Figure S10**), and the reaction solution was allowed to overflow through the upper end (bottom right in **Figure S10**). Using this setup, the liquid output of the hydrogenation reaction could be continuously monitored without any interfering gas bubbles, whilst maintaining a minimal hold-up volume. Additionally, a smaller PTFE tube (0.8 mm o.d., 0.3 mm i.d., 2 × 80 cm length) was used to continuously withdraw a stream for online UHPLC sampling, which is further discussed in section 3.2.1.

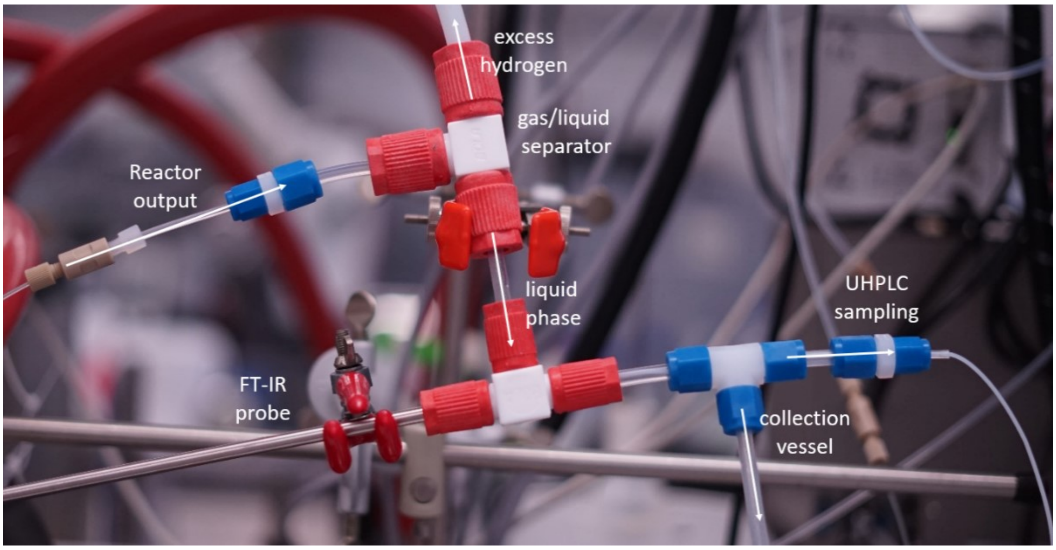

Figure S10. Gas-liquid separator mounted above FT-IR probe, including tubing for UHPLC sampling.

3.1.2. Offline Calibration Procedure

The large number of species were formed in the reaction, many of which were not commercially available and so required offline calibration. Samples containing mixtures of different chemicals were produced in steady-state runs using the Miprowa reactor.

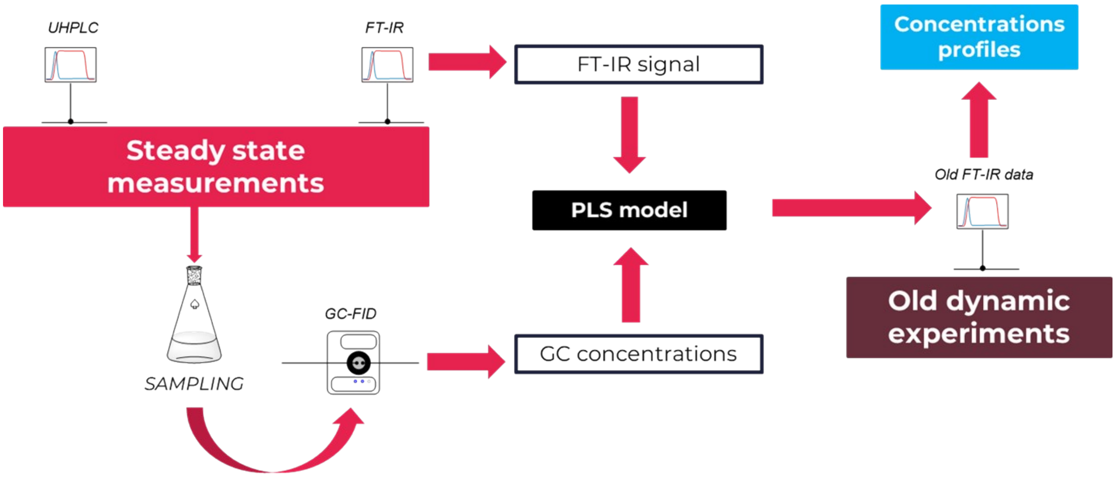

Figure S11. Schematic representation of the data acquisition and calibration approach and application to pre-recorded experimental data.

The GC-FID concentrations of steady state samples were used to calibrate an FT-IR PLS model. The PLS model was then used to reprocess the FT-IR data premeasured in the dynamic experiments, thus obtaining the concentration profile for each species. The data used for calibrations were obtained in two experiments (Experiment 8 and Experiment 9). Details can be found in Section 5.

Table S1. A list of conditions used for steady state experiments for offline calibration.

CSM	Temperature	Liquid flow
	[°C]	[mL/min]
Pt/Al_2O_3	60	0.5
	60	1.5
	60	2.5
	60	4
	80	0.5
	80	1
	80	4
	100	4
	100	0.5
	40	4
	40	1.5
Pd/Al_2O_3	80	2
	80	0.5
	100	0.5
	100	1.5
	120	0.5
	120	1
	120	2
	120	2.5
	120	4

For each sample a minimum of three residence times were allowed before collecting a sample from the reactor outlet. The collected samples were diluted (50 µL in 1 mL acetonitrile) and analyzed by GC-FID. Due to the unavailability of standards, the content of each species was expressed as absolute percentage, without a correction for the response factor.

Table S2. A list of measured relative responses between commercially-available compounds.

Species	Molar mass (mg/mmol)	Concentration (mmol/L)	Area (a.u.)	Response Factor
1	136.15	1.08	18862	1.04
2	138.17	1.05	14751	0.84
3	122.17	1.27	23583	1.11
6	128.22	1.32	20558	0.93
1,3,5 trimethoxybenzene	168.19	0.80	13455	-

It can be seen that no significant difference is present and therefore the error made in taking the factor equal to one for all the species is minor.

3.1.3. Partial Least Squares (PLS) Regression

Due to the large number of species formed in the reaction, the FT-IR signal was analyzed by Partial Least Squares (PLS) regression. PLS regression was performed using the PEAXACT 5.3 software (S-PACT).

Table S3. Calibration summary for each compound. Major species are highlighted.

Species	Calibration Range (mM)	Rank	R^2	$RMSE_C$ (mM)	$RMSE_{CV}$ (mM)	$RMSE_P$ (mM)	Training samples	Test samples
1	2-377	4	0.9994	3.0	4	4	701	199
2	6-190	5	0.9818	6.5	10	6	701	199
3	0-352	4	0.9967	6.6	11	9	701	199
4	0-9	2	0.9646	0.54	0.7	0.4	701	199
5	0-32	3	0.8912	3.0	6	2	701	199
6	0-12	4	0.9103	0.91	2	0.5	701	199
7	0-282	4	0.9958	5.3	8	6	701	199
8	0-8	4	0.9915	0.22	0.3	0.3	701	199
9	0-9	3	0.8738	0.99	2	0.6	701	199

The samples were analyzed with the FT-IR probe inserted in the gas liquid separator. After gathering the spectra, the measurement was paused, the probe cleaned with acetone and dried with argon, then the next sample was measured. The acquired training set spectra were read into PEAXACT in SPC format. For an even better approximation, the PLS model was refined with process data. These data were used for calibration using the concentrations obtained from the GC-FID measurements.

The spectra were processed with the following pre-treatment conditions. Baseline correction: rubber band subtraction; smoothing/derivative: first order derivative. The global range (3400-800 cm-1) was reduced to the interval from 400 to 2400 cm^{-1} to avoid processing parts of the spectrum without relevant information. Additionally, the ranges 1720 to 1790 cm^{-1} and 2050 to 2120 cm^{-1} were neglected due to very intense signals of solvent.

To gain the calibration model, imported spectra were tagged with the "true" concentration values of each compound in the mixture. Due to the large availability of calibration samples, some of which having similar concentrations, the calibration set was split into "training" samples and "test" samples. The former was used to build the calibration model and establish the model statistics (R^2, Root Mean Squared Error of Calibration $RMSE_C$, Root Mean Squared Error of Cross Validation $RMSE_{CV}$). Cross validation (CV) was executed. By dividing the N original training samples into two subsets, one training set to fit the calibration model and one test set to compute a validation error. These sets were re-divided and validated until every sample had been used for testing exactly once. The validation errors were then averaged over the partitions to give the cross-validation error, which reflects the predictive performance of the model. Due to large availability of calibration samples, the method "Leave-group-out" was chosen. For all compounds in every model a rank had to be chosen, reflecting the "degree of fitting" that is applied. The ranks were adjusted considering two factors, namely the observation of the parity plot and minimizing the $RMSE_C$ and the $RMSE_{CV}$. Typically, the number of ranks used in the models varied between 2 and 6. The "test" samples of the original data were instead used to establish the Root Mean Squared Error of Prediction ($RMSE_P$), useful to establish the error of predicted data. To these samples, the calibration model was applied and the error of prediction was computed and reported.

Predicted vs True plots for all component models are shown below:

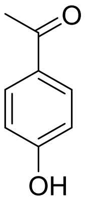

1

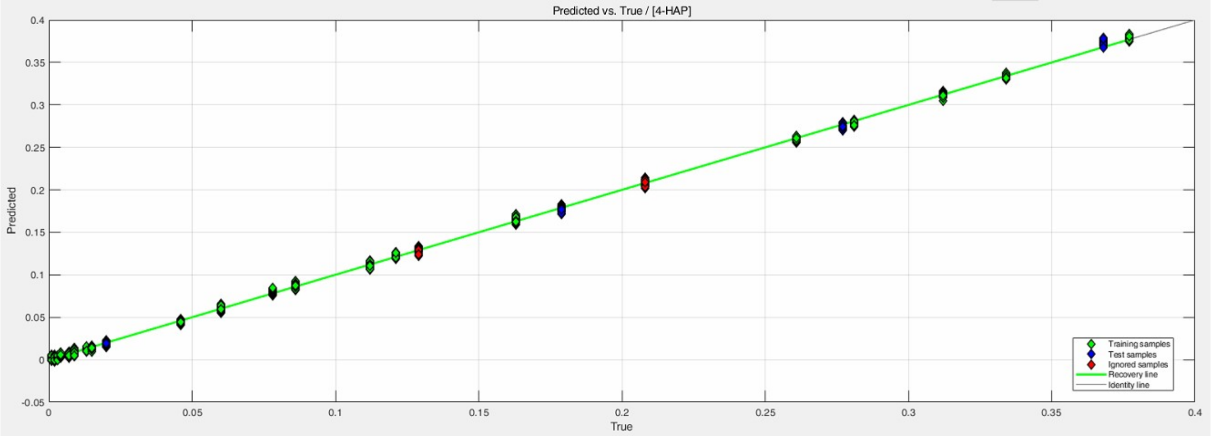

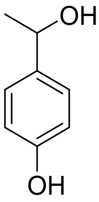

2

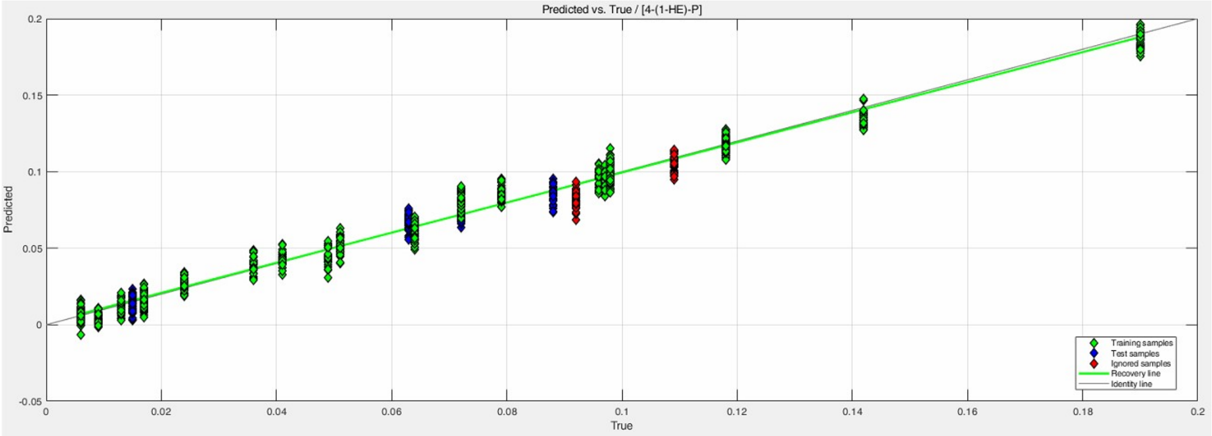
Predicted vs. True / [4-(1-HE)-P]
Predicted
True
0.2
0.15
0.1
0.05
0
-0.05
0
0.02
0.04
0.06
0.08
0.1
0.12
0.14
0.16
0.18
0.2
Training samples
Test samples
Ignored samples
Recovery line
Identity line

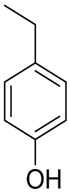

3

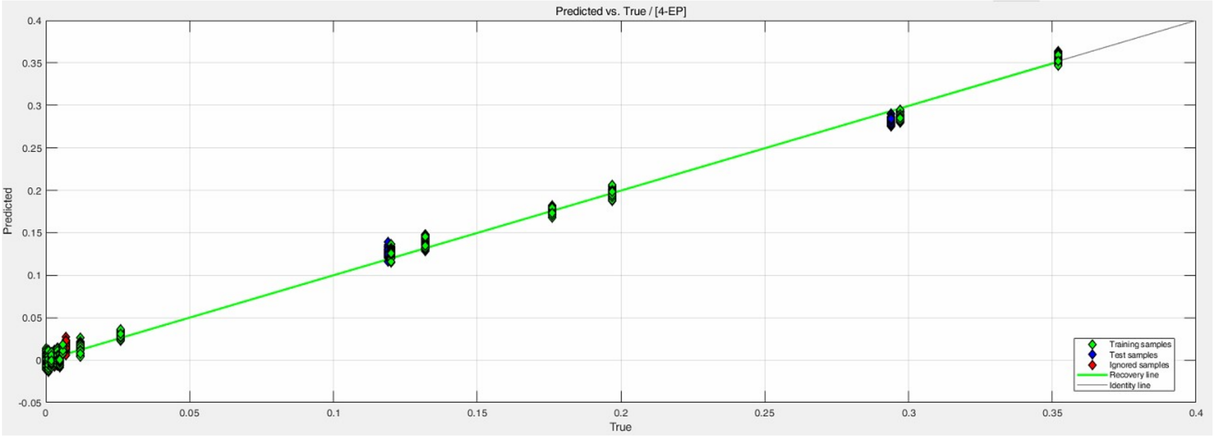
Predicted vs. True / [4-EP]
Predicted
True
0.4
0.35
0.3
0.25
0.2
0.15
0.1
0.05
0
-0.05
0
0.05
0.1
0.15
0.2
0.25
0.3
0.35
0.4
Training samples
Test samples
Ignored samples
Recovery line
Identity line

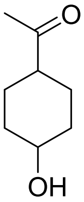
O
OH

4

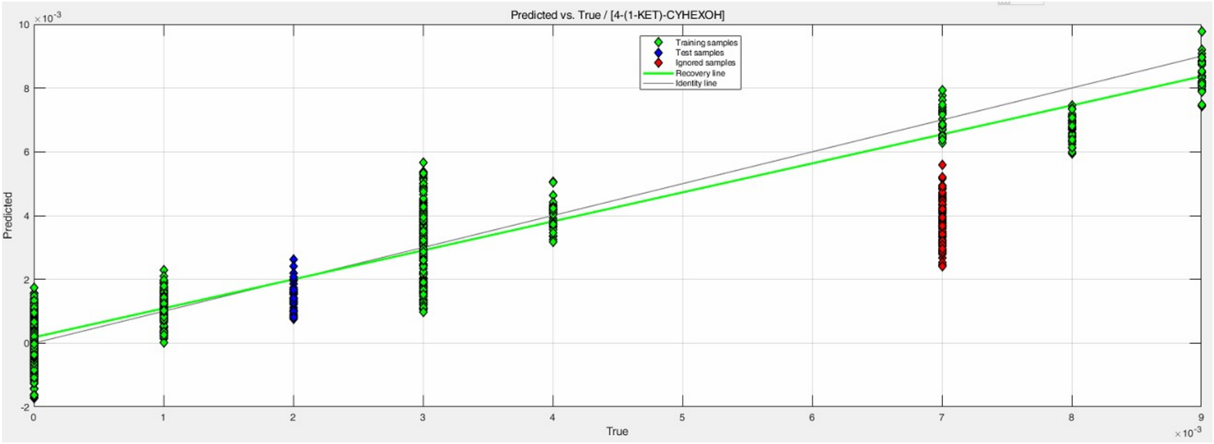
Predicted vs. True / [4-(1-KET)-CYHEXOH]
Training samples
Test samples
Ignored samples
Recovery line
Identity line
Predicted
True
×10^-3
10
8
6
4
2
0
-2
0
1
2
3
4
5
6
7
8
9
×10^-3

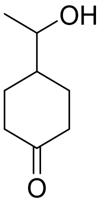
OH
O

5

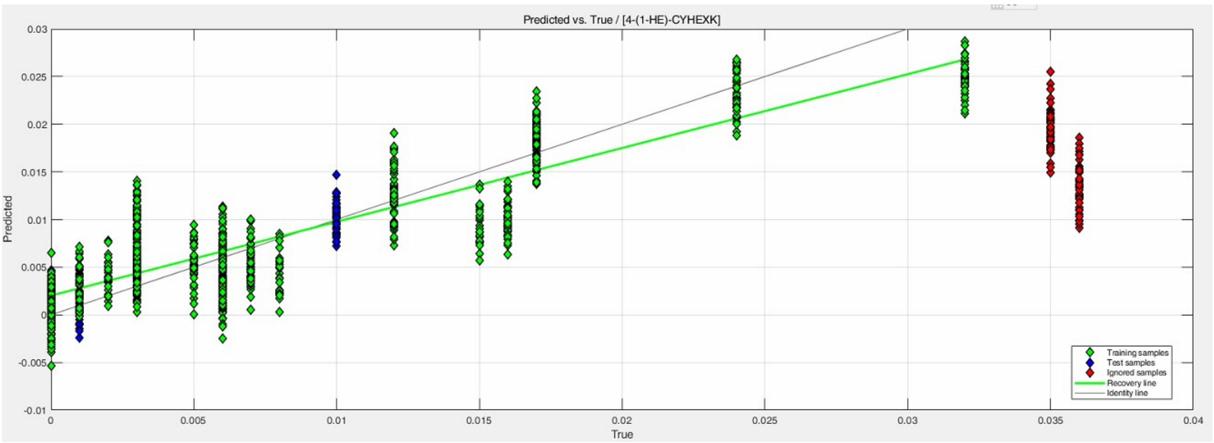
Predicted vs. True / [4-(1-HE)-CYHEXK]
Training samples
Test samples
Ignored samples
Recovery line
Identity line
Predicted
True
0.03
0.025
0.02
0.015
0.01
0.005
0
-0.005
-0.01
0
0.005
0.01
0.015
0.02
0.025
0.03
0.035
0.04

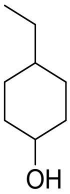
OH

6

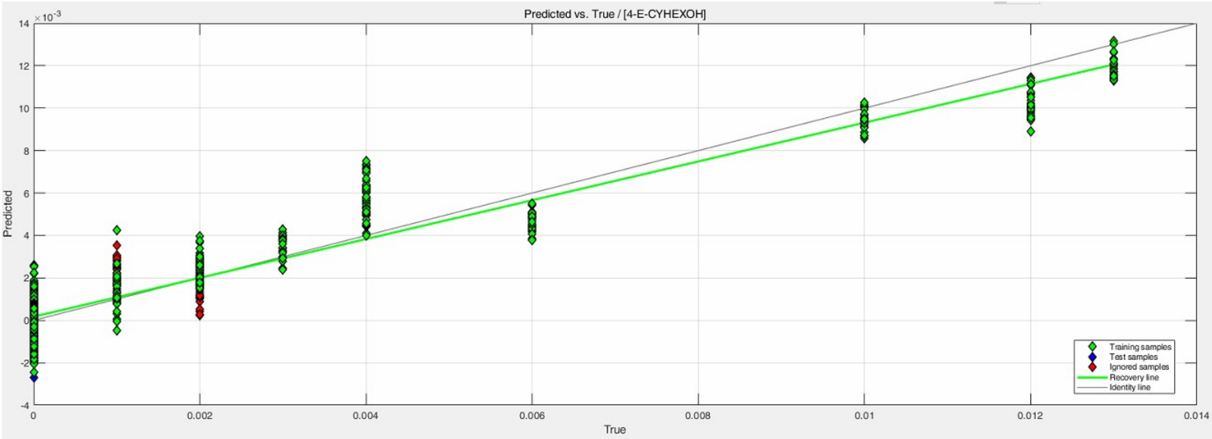
Predicted vs. True / [4-E-CYHEXOH]
×10^-3
14
12
10
8
6
4
2
0
-2
-4
Predicted
0
0.002
0.004
0.006
0.008
0.01
0.012
0.014
True
Training samples
Test samples
Ignored samples
Recovery line
Identity line

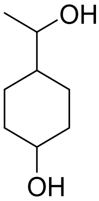
OH
OH

7

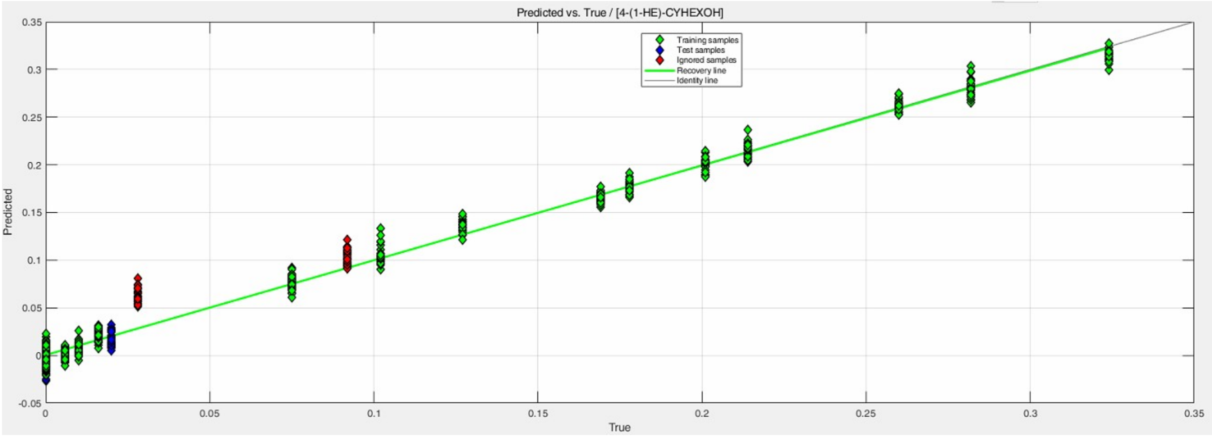
Predicted vs. True / [4-(1-HE)-CYHEXOH]
0.35
0.3
0.25
0.2
0.15
0.1
0.05
0
-0.05
Predicted
0
0.05
0.1
0.15
0.2
0.25
0.3
0.35
True
Training samples
Test samples
Ignored samples
Recovery line
Identity line

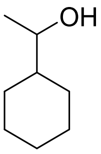

8

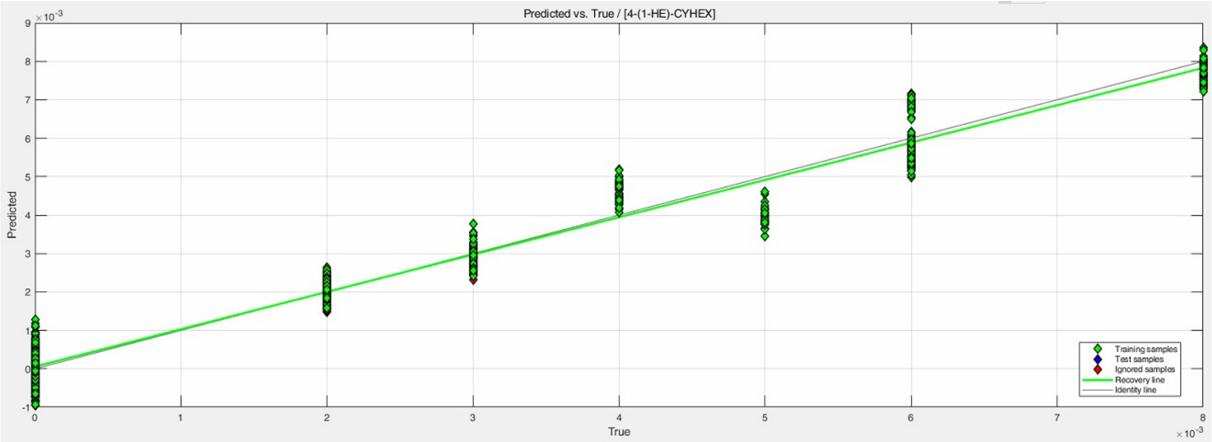

Predicted vs. True / [4-(1-HE)-CYHEX]
×10^-3
Predicted
True
×10^-3
9
8
7
6
5
4
3
2
1
0
-1
0
1
2
3
4
5
6
7
8
Training samples
Test samples
Ignored samples
Recovery line
Identity line

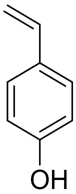

9

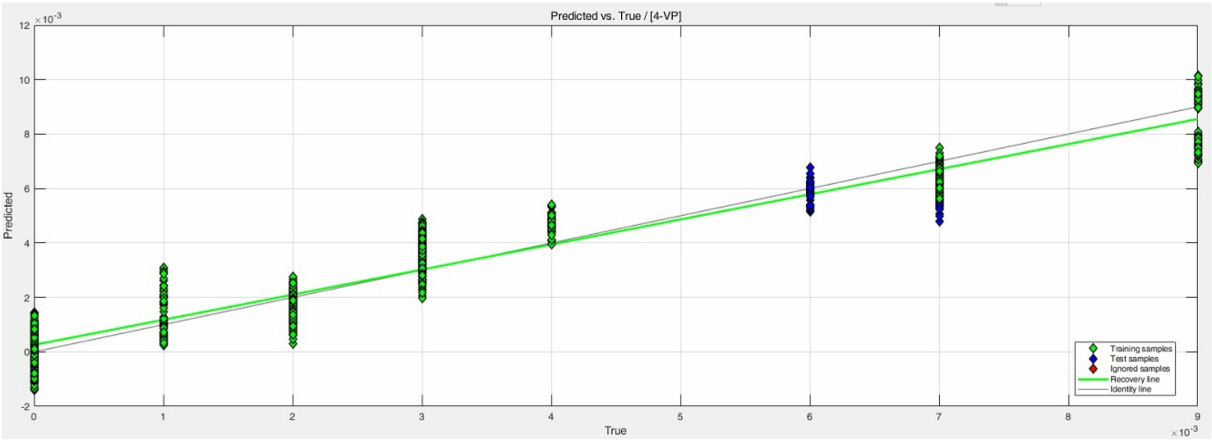

Predicted vs. True / [4-VP]
×10^-3
Predicted
True
×10^-3
12
10
8
6
4
2
0
-2
0
1
2
3
4
5
6
7
8
9
Training samples
Test samples
Ignored samples
Recovery line
Identity line

3.2. Online UHPLC Analysis

3.2.1. General

The UHPLC-DAD was comprised of a degassing unit (DGU-20A), two solvent delivery units (LC-30AD), a thermoregulated autosampler (SIL-30AD), thermoregulated column oven (CTO-20AC), diode array detector (SPD-M30A) and a control unit (CBM-20A).

Analysis was performed using a Phenomenex Luna Omega C18 column (50 × 2.1 mm, particle size 1.6 µm, pore size 100 Å) at 45 °C using mobile phase A (H_2O + 0.01% CF_3COOH) and B (MeCN + 0.01% CF_3COOH) at a total flow rate of 1 mL/min. The column was exchange with a new column of the same type, due to degrading performance, between run 18 and run 20.

The mobile phases A and B were prepared from HPLC grade solvents.

Compounds were eluted with the following method: starting with 5% B for 0.1 min, increasing to 15.8 % B over 0.65 min, increasing to 100 % B over 1 min, holding 100 % B for 0.5 min, then decreasing B to 5% in 0.01 min and holding for 1 min at 5% to equilibrate the column (3.25 min total acquisition time). Chromatograms were integrated at a wavelength of 215 nm.

Figure S12. Overview of the gradient in the employed online UHPLC method.

3.2.2. Calibration

Substrate **1**, products **2** and **3** were calibrated with an external calibration method and also with an internal standard calibration method using biphenyl ether as an internal standard (ISTD) by UHPLC. For these calibrations, 5 mixtures of varying compound concentrations were prepared by the following procedure:

A 16 mM ISTD stock solution was prepared by weighing in the appropriate amount of ISTD in a 100 mL volumetric flask. The flask was filled up with ethyl acetate to the mark. The compounds to be calibrated were weighed in in 5 mL volumetric flasks and filled to the mark with the ISTD stock solution. The concentrations in mol/L of the five calibration mixtures are in **Table S4**. The calibration was performed twice during the experimental campaign, using the same solutions.

Table S4. Summary of compounds and solutions used to calibrate the UHPLC method.

Compound number	Retention time (min)	Conc. in Solution 1 (mol/L)	Conc. in Solution 2 (mol/L)	Conc. in Solution 3 (mol/L)	Conc. in Solution 4 (mol/L)	Conc. in Solution 5 (mol/L)
1	0.837	0.407	0.318	0.222	0.105	0.037
2	0.472	0.039	0.104	0.203	0.308	0.407
3	1.396	0.035	0.077	0.149	0.231	0.301

The calibration was run using absolute areas, due to the high reproducibility of injection volumes using the internal sample injector. The fitting for the three compounds was performed using the Shimadzu Lab Solutions Lite software with a linear fit forced through 0. The calibration curves for the two calibrations are shown below.

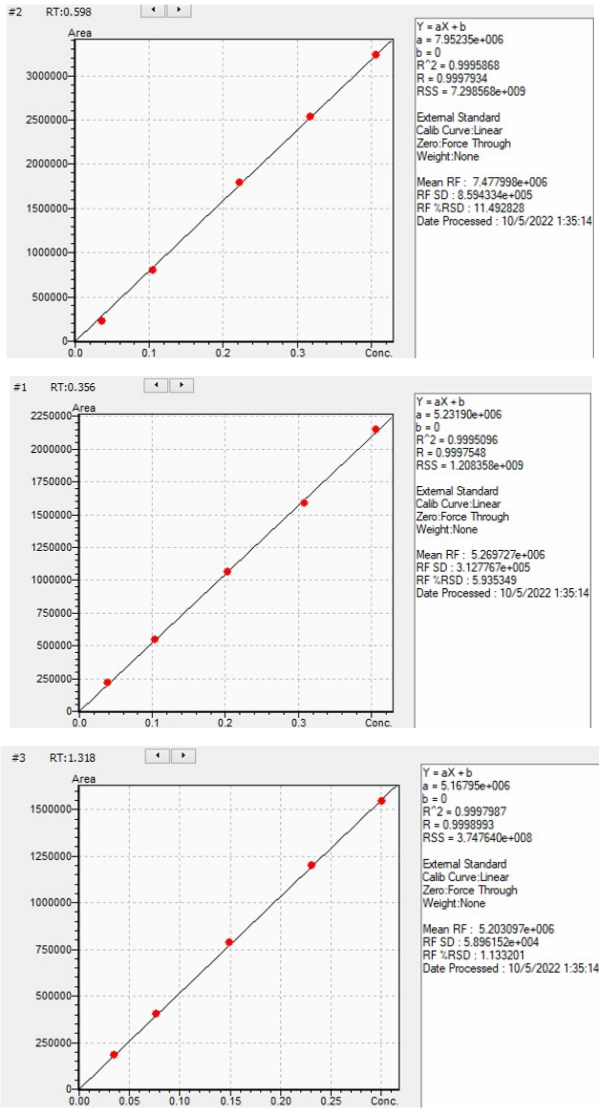

```
Y = aX + b
a = 7.95235e+006
b = 0
R^2 = 0.9995868
R = 0.9997934
RSS = 7.298568e+009

External Standard
Calib Curve:Linear
Zero:Force Through
Weight:None

Mean RF :  7.477998e+006
RF SD : 8.594334e+005
RF %RSD : 11.492828
Date Processed : 10/5/2022 1:35:14
```

```
Y = aX + b
a = 5.23190e+006
b = 0
R^2 = 0.9995096
R = 0.9997548
RSS = 1.208358e+009

External Standard
Calib Curve:Linear
Zero:Force Through
Weight:None

Mean RF :  5.269727e+006
RF SD : 3.127767e+005
RF %RSD : 5.935349
Date Processed : 10/5/2022 1:35:14
```

```
Y = aX + b
a = 5.16795e+006
b = 0
R^2 = 0.9997987
R = 0.9998993
RSS = 3.747640e+008

External Standard
Calib Curve:Linear
Zero:Force Through
Weight:None

Mean RF :  5.203097e+006
RF SD : 5.896152e+004
RF %RSD : 1.133201
Date Processed : 10/5/2022 1:35:14
```

Figure S13. UHPLC calibration A for, from top to bottom, substrate 1, products 2, and 3.

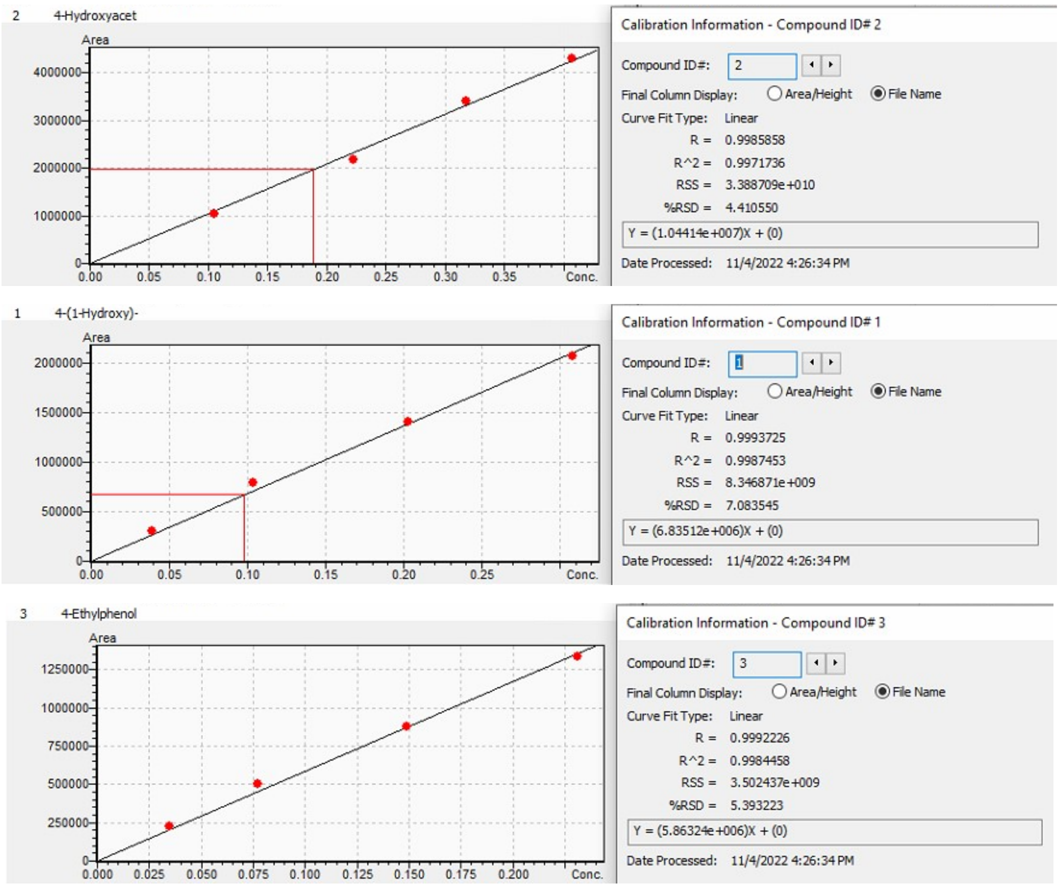

Calibration Information - Compound ID# 2

Compound ID#: 2

Final Column Display: ○ Area/Height ● File Name

Curve Fit Type: Linear

R = 0.9985858

R^2 = 0.9971736

RSS = 3.388709e+010

%RSD = 4.410550

Y = (1.04414e+007)X + (0)

Date Processed: 11/4/2022 4:26:34 PM

Calibration Information - Compound ID# 1

Compound ID#: 1

Final Column Display: ○ Area/Height ● File Name

Curve Fit Type: Linear

R = 0.9993725

R^2 = 0.9987453

RSS = 8.346871e+009

%RSD = 7.083545

Y = (6.83512e+006)X + (0)

Date Processed: 11/4/2022 4:26:34 PM

Calibration Information - Compound ID# 3

Compound ID#: 3

Final Column Display: ○ Area/Height ● File Name

Curve Fit Type: Linear

R = 0.9992226

R^2 = 0.9984458

RSS = 3.502437e+009

%RSD = 5.393223

Y = (5.86324e+006)X + (0)

Date Processed: 11/4/2022 4:26:34 PM

Figure S14. UHPLC calibration B for, from top to bottom, substrate 1, products 2, and 3.

3.2.3. Process Integration

Online UHPLC analysis was possible by using an UHPLC internal sample injector (10 nL, 20000 psi, Cheminert Nanovolume, Part# C84U-6674-.01EUH), which was controlled by the Shimadzu LabSolutions software. The injection valve was triggered according to the following pattern, defined within the acquisition method: 0.01 min inject; 6.00 min load. Samples were continuously withdrawn as a bypass directly after the FT-IR probe and pumped through the injection valve using PTFE tubing (0.3 mm i.d.) with a total volume of 112 µL. A peristaltic pump (Vapourtec SF-10) was used to pump the product stream with a constant flow rate of 500 µL/min.

4. Experimental Details

4.1. Preparation of Feed Solutions

Feed solutions were freshly prepared before each flow ramp experiment. 1-(4-Hydroxyphenyl)-ethanone **1** (Sigma Aldrich, 99%) was dissolved in ethyl acetate (1 L, VWR, 99.8%) and then filtered through filter paper. Solution concentration was measured using the online injection system of the UHPLC and the method normally used for analyzing the data.

4.2. Standard reaction procedure

Before the run was started, the system was flushed with ethyl acetate for at least 30 min. During this time the FT-IR was filled with liquid nitrogen and left to equilibrate for at least 1 h. The reactor was then brought to the starting temperature using a liquid flow rate of 0.5 mL/min. Upon reaching the reaction temperature, the system was pressurized with liquid and then hydrogen was introduced at a constant flow rate of 36 NmL/min. This flow rate was chosen to ensure that hydrogen is not the limiting factor in the system. At the same time the FT-IR recording was started. The system was left to equilibrate for at least 30 min. The solution of solvent was then replaced with that of the solution of starting material. Once the steady state was reached in the IR signal, the dynamic experiment was started. This comprises the following steps

- 10 min at constant liquid flow rate of 0.5 mL/min
- 30 min liquid flow ramp from 0.5 mL/min to 4 mL/min
- 10 min at constant liquid flow rate of 4 mL/min
- 30 min liquid flow ramp from 4 mL/min to 0.5 mL/min
- 10 min at constant liquid flow rate of 0.5 mL/min

Following the last step, the temperature was increased rapidly to the next temperature and the system was left to equilibrate for 20 min. After equilibration at the new temperature the procedure was repeated for the new temperature.

Once the reaction was complete the system was purged with ethyl acetate until the FT-IR signal showed no sign of remaining chemicals in the system and cooled down under a flow of hydrogen. Once temperature dropped below 60 °C, pressure was released and the recording stopped. The experiments were carried out at high pressure (20 bar) to ensure a full saturation of the catalyst surface was obtained, thus simplifying the kinetic expression.

4.3. Process control

4.3.1. Software

The entire platform (aside from the peristaltic pump leading to the UHPLC) was monitored and controlled using a HiTec Zang LabManager and LabVision software (**Figure S15**). Actuators were automated according to **Table S5**.

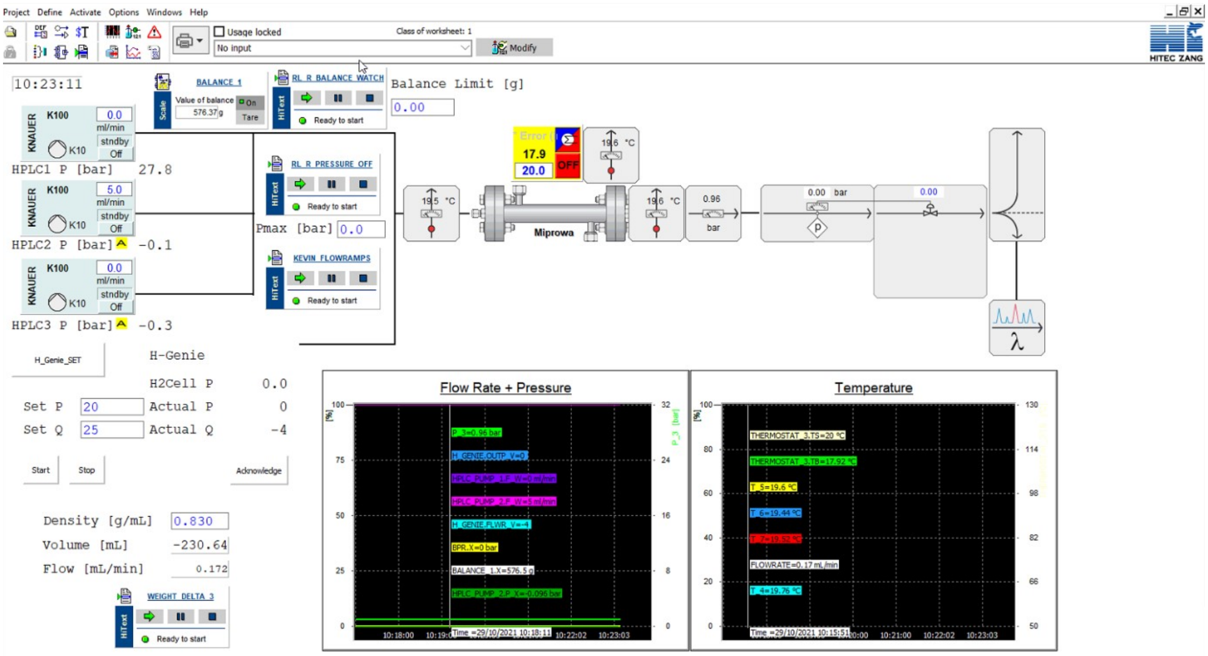

No input

10:23:11

Value of balance 576.37 g

Ready to start

Balance Limit [g] 0.00

K100 0.0 ml/min

HPLC1 P [bar] 27.8

K100 5.0 ml/min

HPLC2 P [bar] -0.1

K100 0.0 ml/min

HPLC3 P [bar] -0.3

Pmax [bar] 0.0

H-Genie

H2Cell P 0.0

Set P 20 Actual P 0

Set Q 25 Actual Q -4

Density [g/mL] 0.830

Volume [mL] -230.64

Flow [mL/min] 0.172

17.9

20.0

19.6 °C

19.5 °C

19.6 °C

0.96 bar

0.00 bar

0.00

P_3=0.96 bar

H_GENIE.OUTP_V=0

HPLC_PUMP_1.F_W=0 ml/min

HPLC_PUMP_2.F_W=5 ml/min

H_GENIE.FLWR_V=-4

BPR.X=0 bar

BALANCE_1.X=576.5 g

HPLC_PUMP_2.P_X=-0.096 bar

Time =29/10/2021 10:18:11

THERMOSTAT_3.TS=20 °C

THERMOSTAT_3.TB=17.92 °C

T_5=19.6 °C

T_6=19.44 °C

T_7=19.52 °C

FLOWRATE=0.17 mL/min

T_4=19.76 °C

Time =29/10/2021 10:15:51

Figure S15. Screenshot of the LabVision software used to control the flow platform.

Table S5. List of equipment that was used in the study and its interface to LabVision.

Instrument Type	Make/Model	Quantity	Interface to LabVision
T sensor	Ehrfeld, 0518-2-1004-X	2	M8
T sensor	Huber, Pt100 M16x1 HUB-6352	1	M8
P sensor	Ehrfeld, 0518-1-60x4-F	1	DIN 5-pin
Pump (HPLC)	Knauer, Azura P 4.1S	2	RS232, NAMUR
Pressure regulator	Bronkhorst, EL-PRESS	1	RS232, NAMUR
H_2 generator	Thales Nano Energy, H-Genie	1	RS232, NAMUR
Thermostat	Huber, CC-304	1	RS232, NAMUR
Balance	Kern, KB 2400-2N	1	RS232, NAMUR

4.3.2. Flow and Temperature Ramps

Full automation of the process and the individual steps to the reaction was achieved using an automated flow ramp protocol. The script written in HiText communicates with the HiTec Zang LabManager and enabled automated ramping of the flow rates (Figure S19). A chosen number of ramp could be implemented in the script. Temperature changes were also implemented.

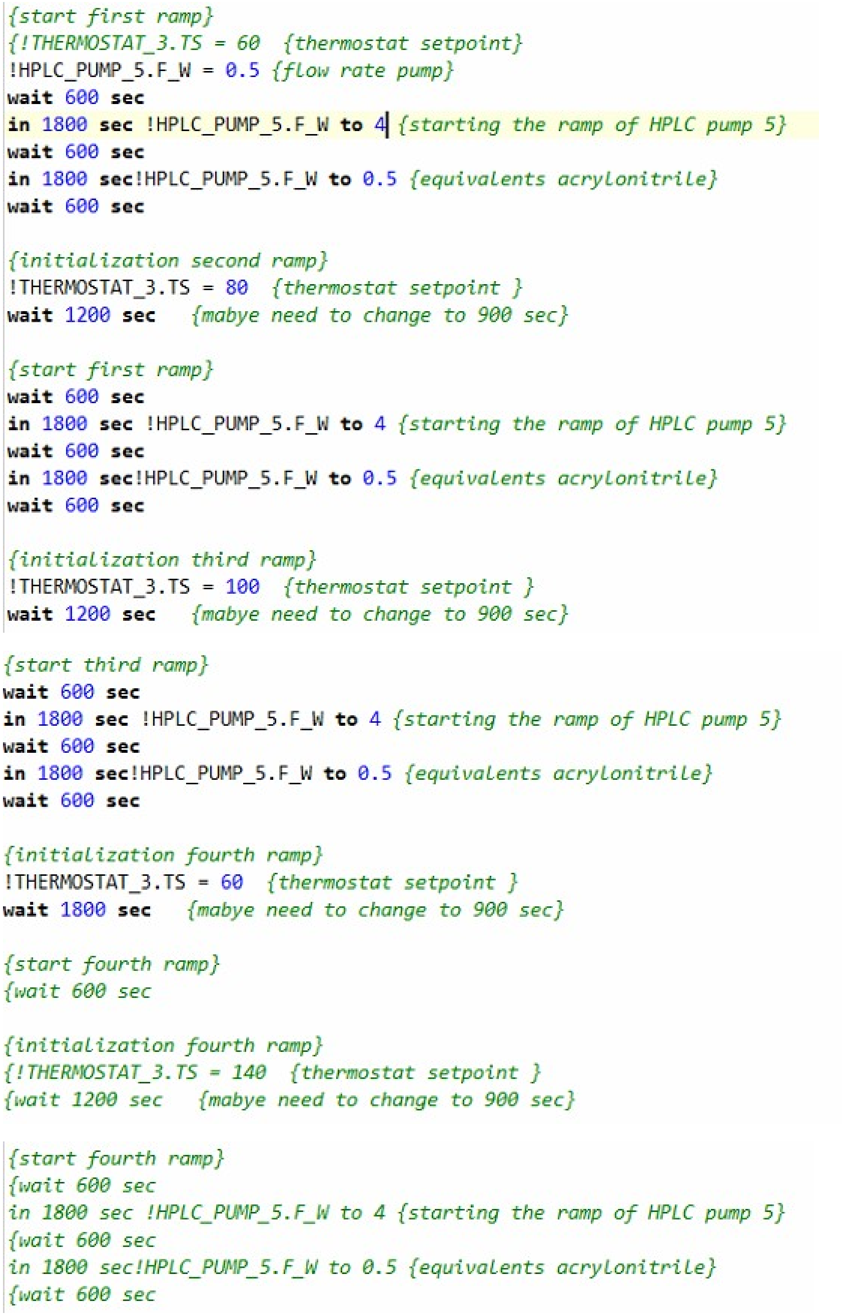

```
{start first ramp}
{!THERMOSTAT_3.TS = 60  {thermostat setpoint}
!HPLC_PUMP_5.F_W = 0.5 {flow rate pump}
wait 600 sec
in 1800 sec !HPLC_PUMP_5.F_W to 4 {starting the ramp of HPLC pump 5}
wait 600 sec
in 1800 sec!HPLC_PUMP_5.F_W to 0.5 {equivalents acrylonitrile}
wait 600 sec

{initialization second ramp}
!THERMOSTAT_3.TS = 80  {thermostat setpoint }
wait 1200 sec   {mabye need to change to 900 sec}

{start first ramp}
wait 600 sec
in 1800 sec !HPLC_PUMP_5.F_W to 4 {starting the ramp of HPLC pump 5}
wait 600 sec
in 1800 sec!HPLC_PUMP_5.F_W to 0.5 {equivalents acrylonitrile}
wait 600 sec

{initialization third ramp}
!THERMOSTAT_3.TS = 100  {thermostat setpoint }
wait 1200 sec   {mabye need to change to 900 sec}

{start third ramp}
wait 600 sec
in 1800 sec !HPLC_PUMP_5.F_W to 4 {starting the ramp of HPLC pump 5}
wait 600 sec
in 1800 sec!HPLC_PUMP_5.F_W to 0.5 {equivalents acrylonitrile}
wait 600 sec

{initialization fourth ramp}
!THERMOSTAT_3.TS = 60  {thermostat setpoint }
wait 1800 sec   {mabye need to change to 900 sec}

{start fourth ramp}
{wait 600 sec

{initialization fourth ramp}
{!THERMOSTAT_3.TS = 140  {thermostat setpoint }
{wait 1200 sec   {mabye need to change to 900 sec}

{start fourth ramp}
{wait 600 sec
in 1800 sec !HPLC_PUMP_5.F_W to 4 {starting the ramp of HPLC pump 5}
{wait 600 sec
in 1800 sec!HPLC_PUMP_5.F_W to 0.5 {equivalents acrylonitrile}
{wait 600 sec
```

Figure S16. HiText code for flow and temperature ramps

5. Experimental Results

Table S6. Summary of experiments performed.

Experiment Number	**CSM type**	**Input Concentration (mol/L)**	**Temperature Levels (°C)**
1	Pd/Al_2O_3	0.400	80, 100, 120, 140
2	Pd/Al_2O_3	0.396	80, 100, 120, 140
3	Ru/Al_2O_3	0.385	80, 100, 120, 80
4	Ru/Al_2O_3	0.398	80, 100, 120, 80
5	Pt/Al_2O_3	0.201	60, 80, 100
6	Pt/Al_2O_3	0.300	60, 80, 100
7	Pt/Al_2O_3	0.400	60, 80, 100, 60
8	Pt/Al_2O_3	0.383	Steady state experiments - tabulated below
9	Pd/Al_2O_3	0.394	Steady state experiments - tabulated below
10	Pd/Al_2O_3	0.401	120
11	Pt/Al_2O_3	0.401	100, 120
12	Pt/Al_2O_3	0.402	100

Table S7. Key to compound numbers. Note: Pairs of diastereomers were treated as a single compound.

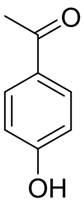	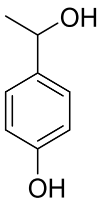	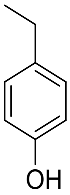	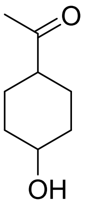	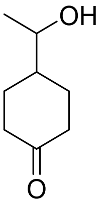	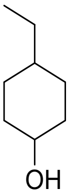	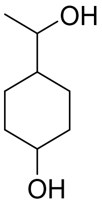	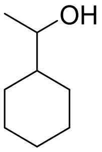	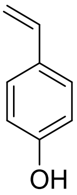
1	**2**	**3**	**4**	**5**	**6**	**7**	**8**	**9**

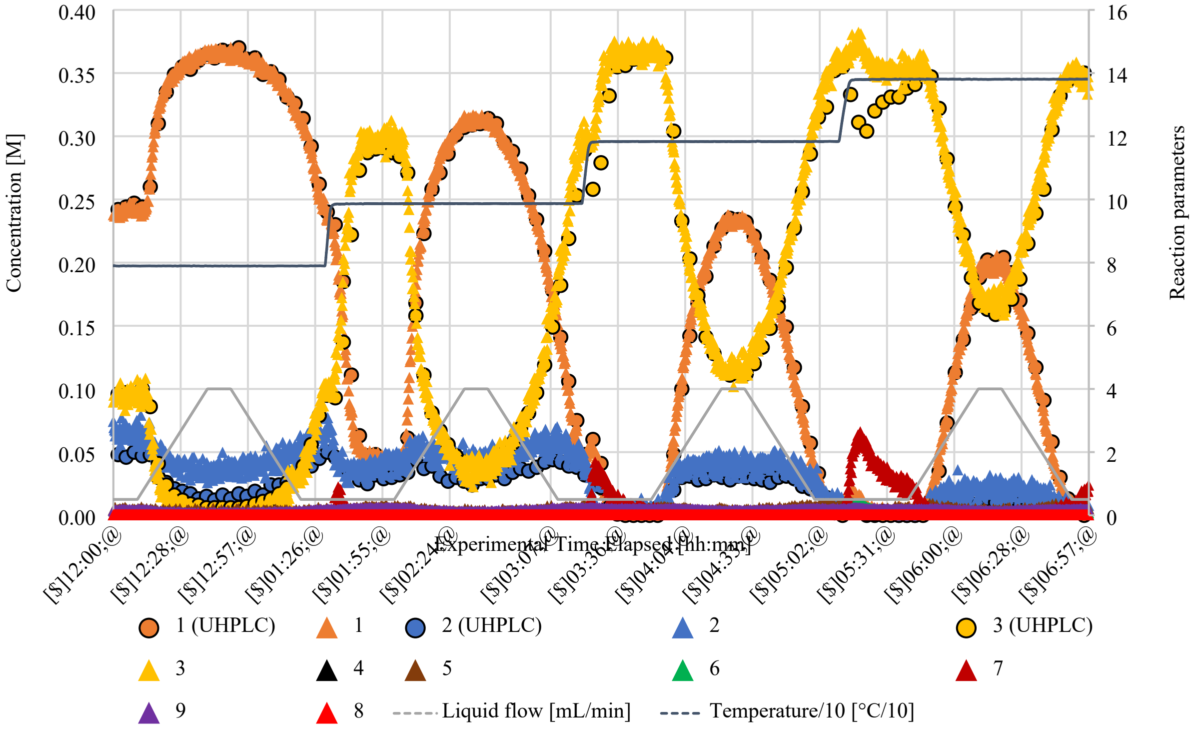

Figure S17. Reaction profile for *Experiment 1*.

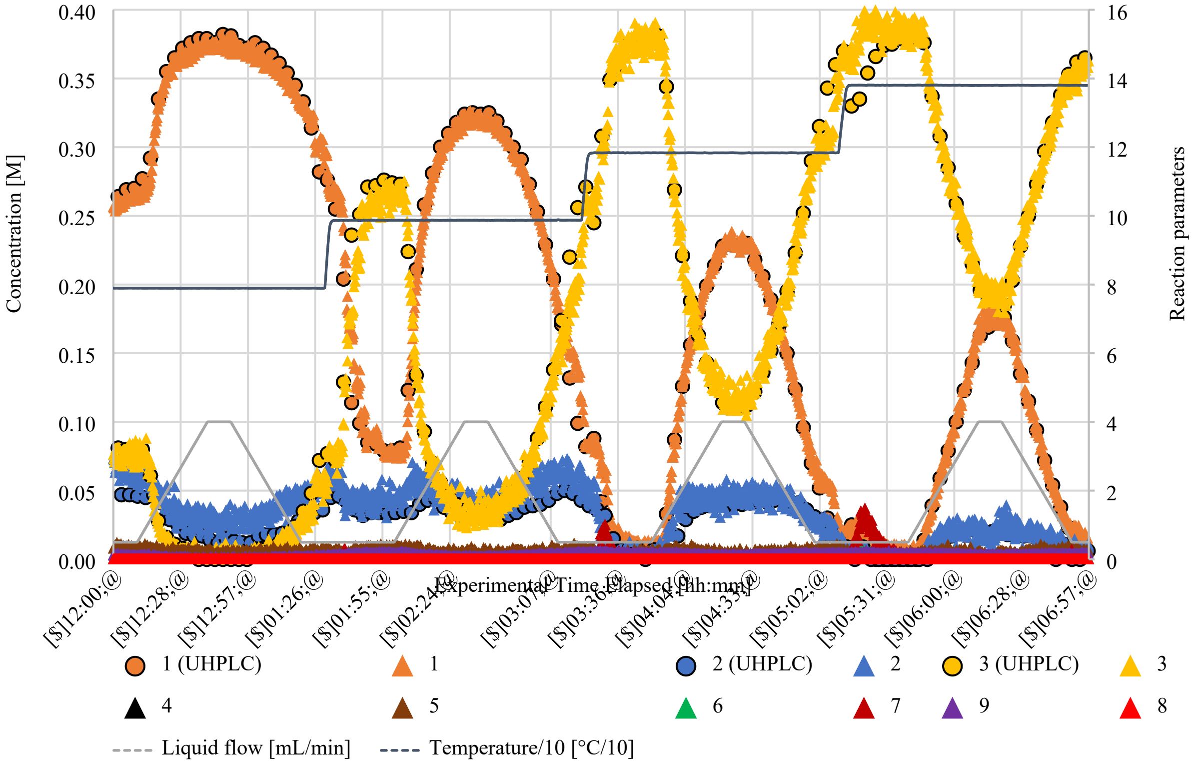

Figure S18. Reaction profile for *Experiment 2*.

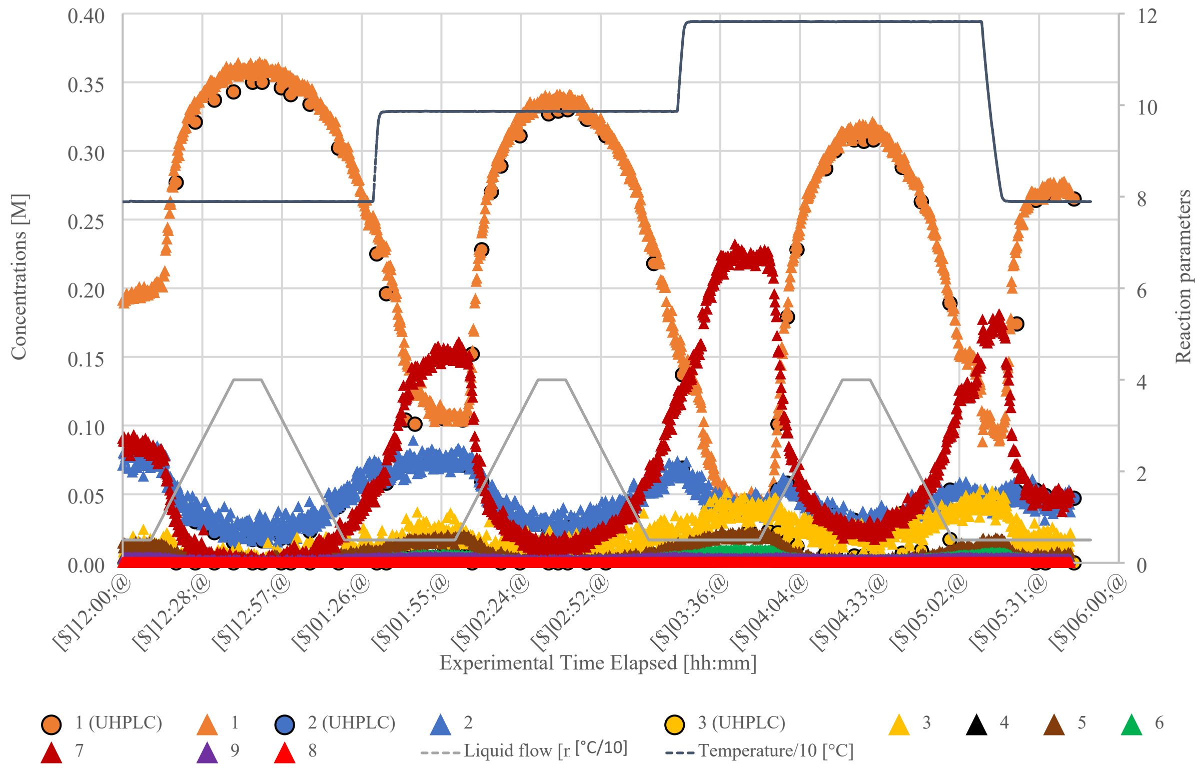

Figure S19. Reaction profile for *Experiment 3*.

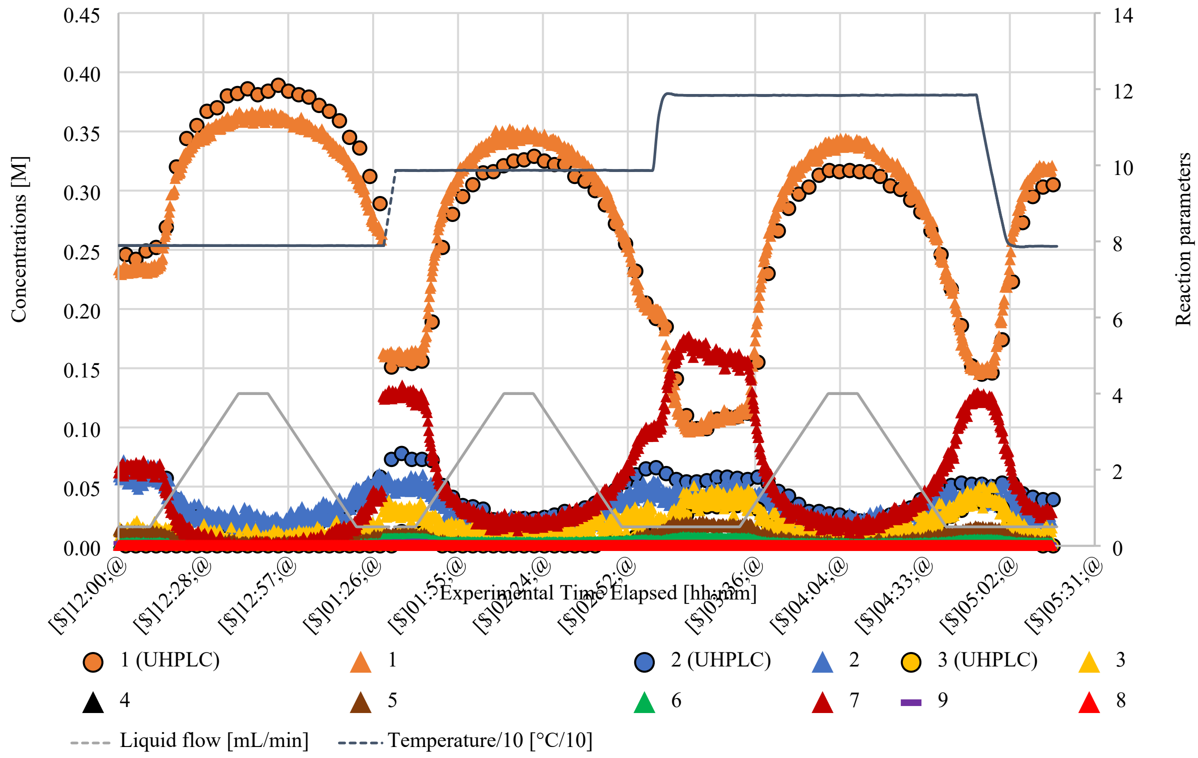

Figure S20. Reaction profile for *Experiment 4*.

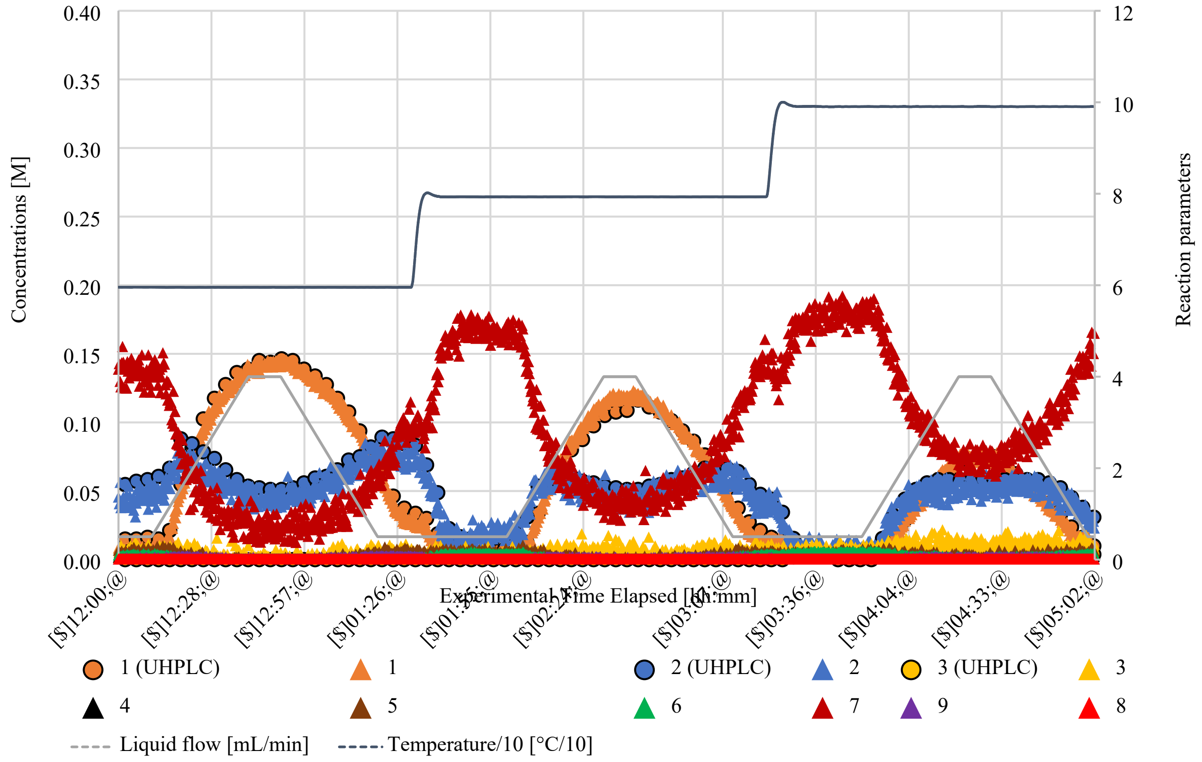

Figure S21. Reaction profile for *Experiment 5*.

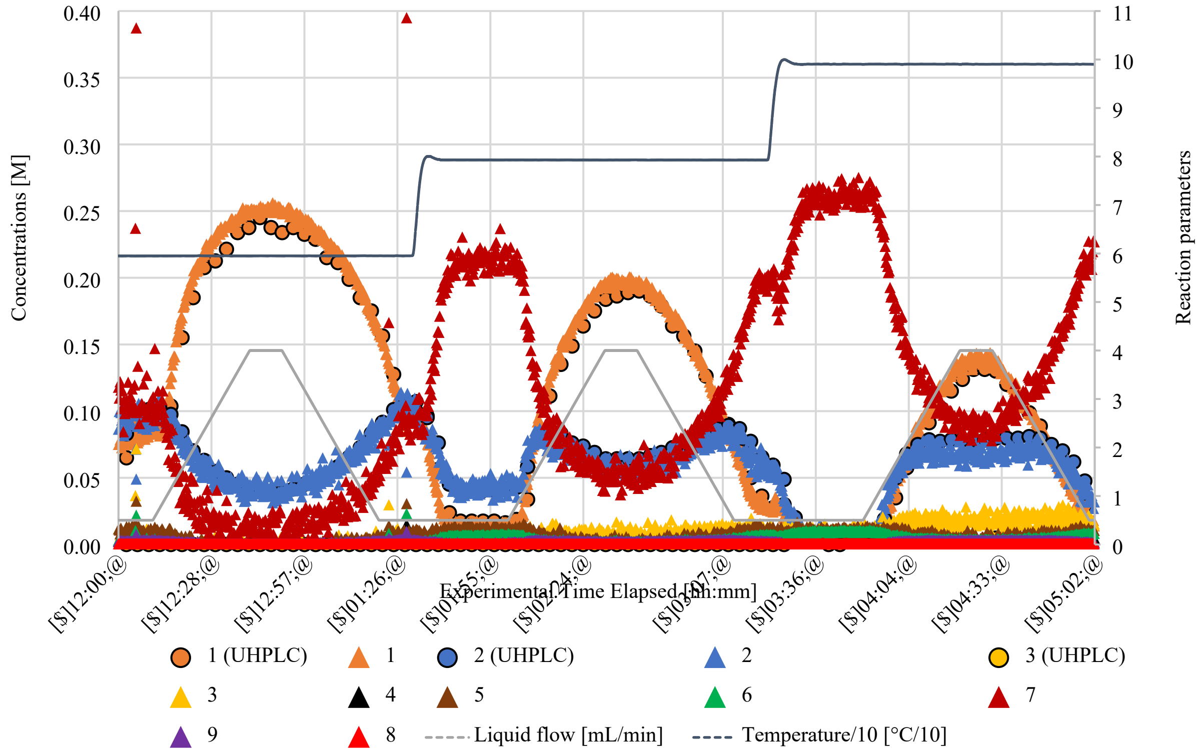

Figure S22. Reaction profile for *Experiment 6*.

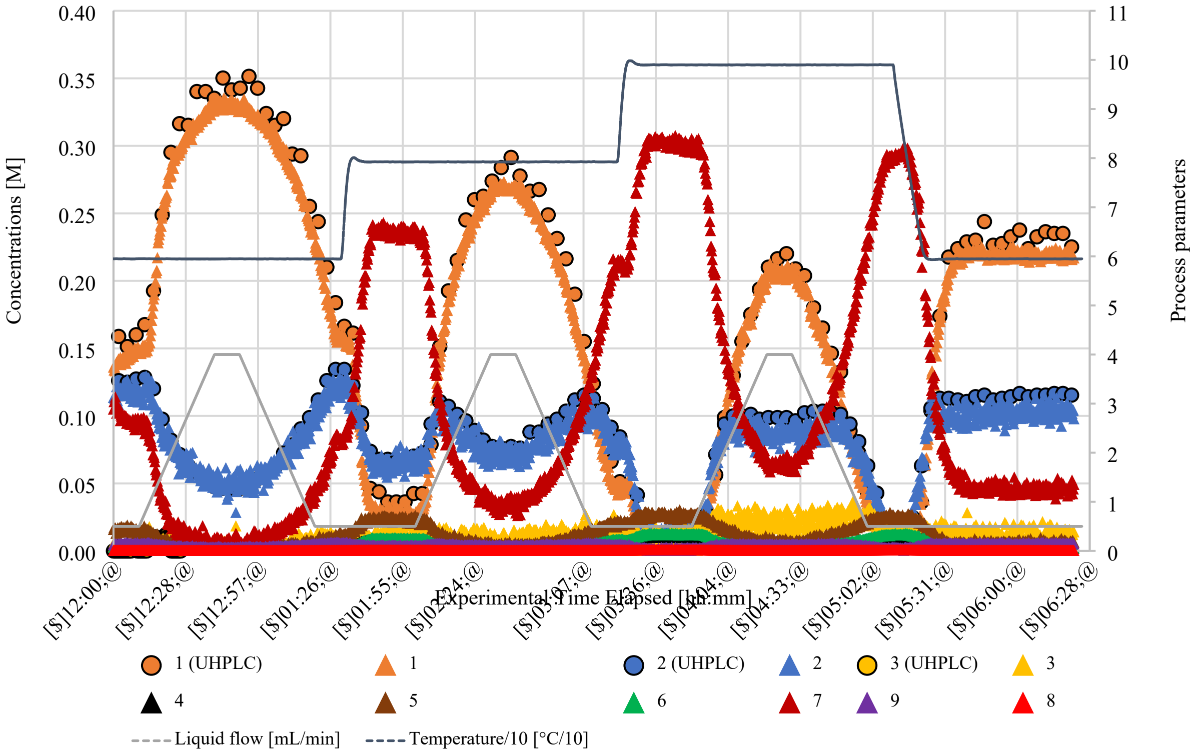

Figure S23. Reaction profile for *Experiment 7*.

Experiment 8 was used to produce the samples for the calibration of the FT-IR probe. The tests performed are reported in table and in figure are the results for the concentrations of the different species. For these tests the system was left to equilibrate at steady state for at least three reactor volumes before the sample was collected.

Test	Temperature [°C]	Liquid flow [mL/min]
1	60	0.5
2	60	1.5
3	60	2.5
4	60	4
5	80	0.5
6	80	1
7	80	4
8	100	4
9	100	0.5
10	40	4
11	40	1.5

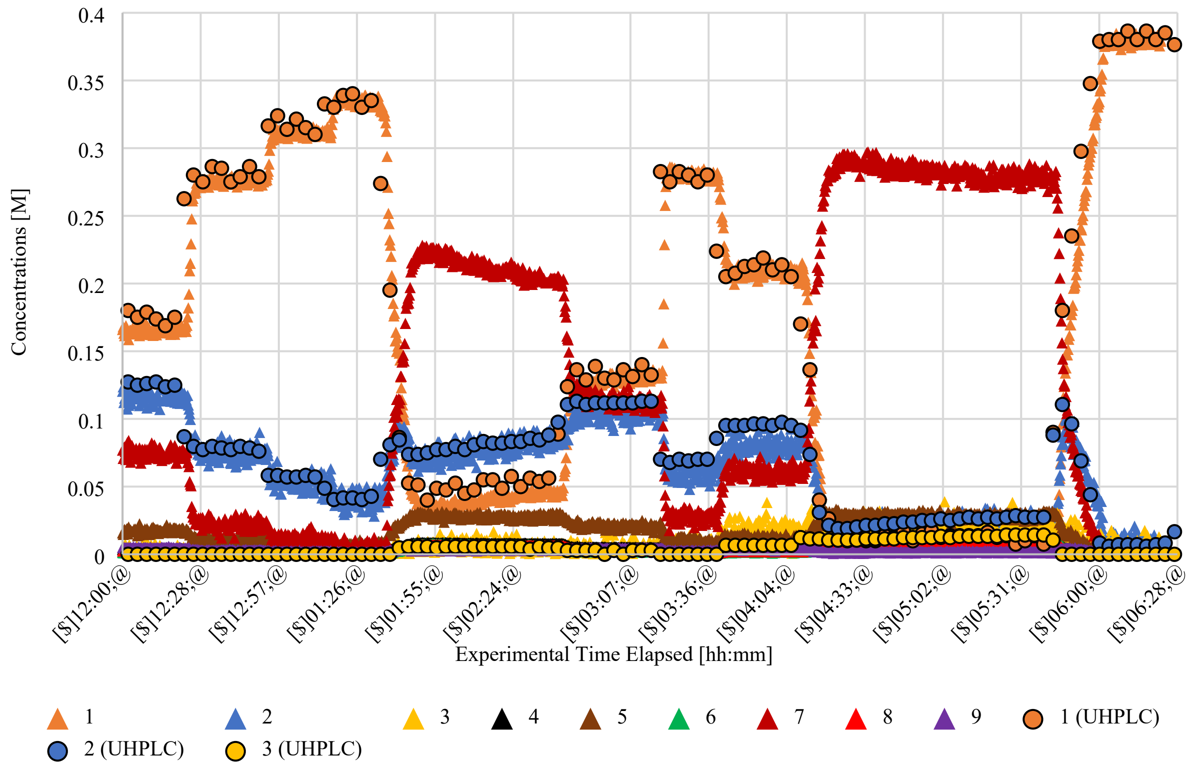

Figure S24. Reaction profile for *Experiment 8*.

The data from Experiment 9 were used for the calibration of the FT-IR.

Test	Temperature [°C]	Liquid flow [mL/min]
1	80	2
2	80	0.5
3	100	0.5
4	100	1.5
5	120	0.5
6	120	1
7	120	2
8	120	2.5
9	120	4

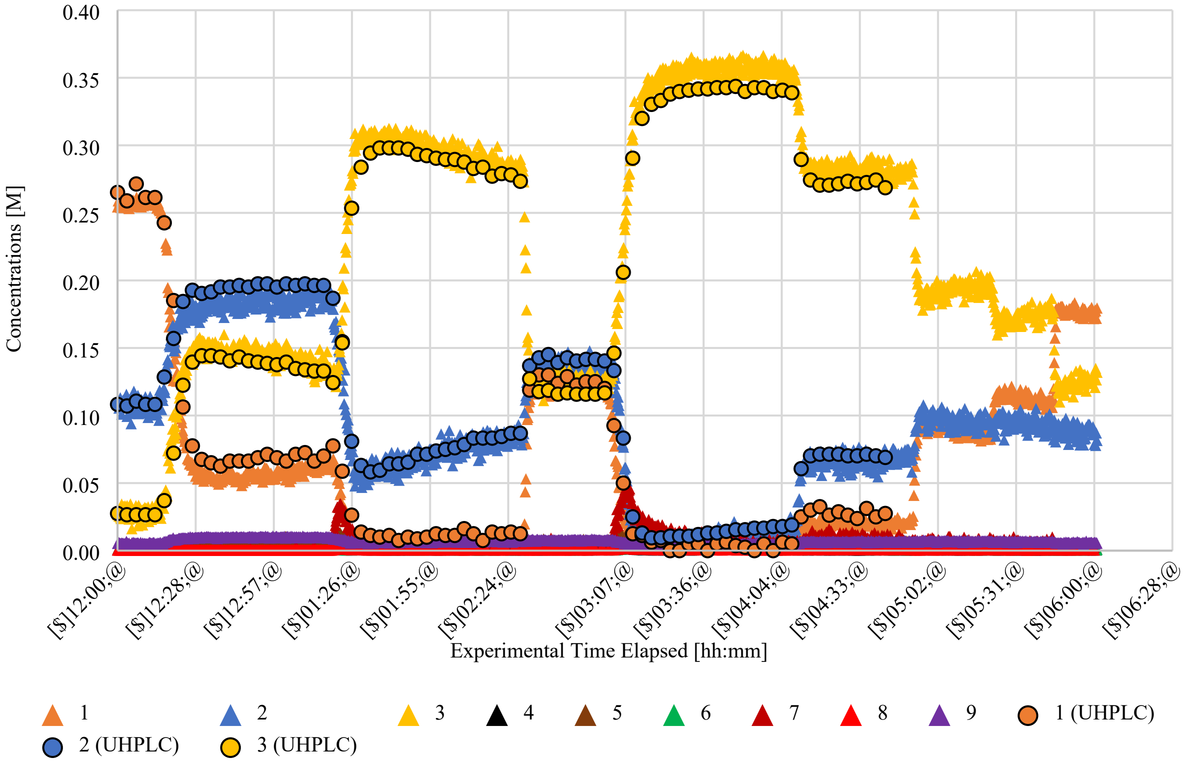

Figure S25. Reaction profile for *Experiment 9.*

Experiment 10 was used to assess the effect of gas flow on the reaction performance. As shown in the figure below, the gas flow rate was changed between 38 and 144 NmL/min without significant change in the performance.

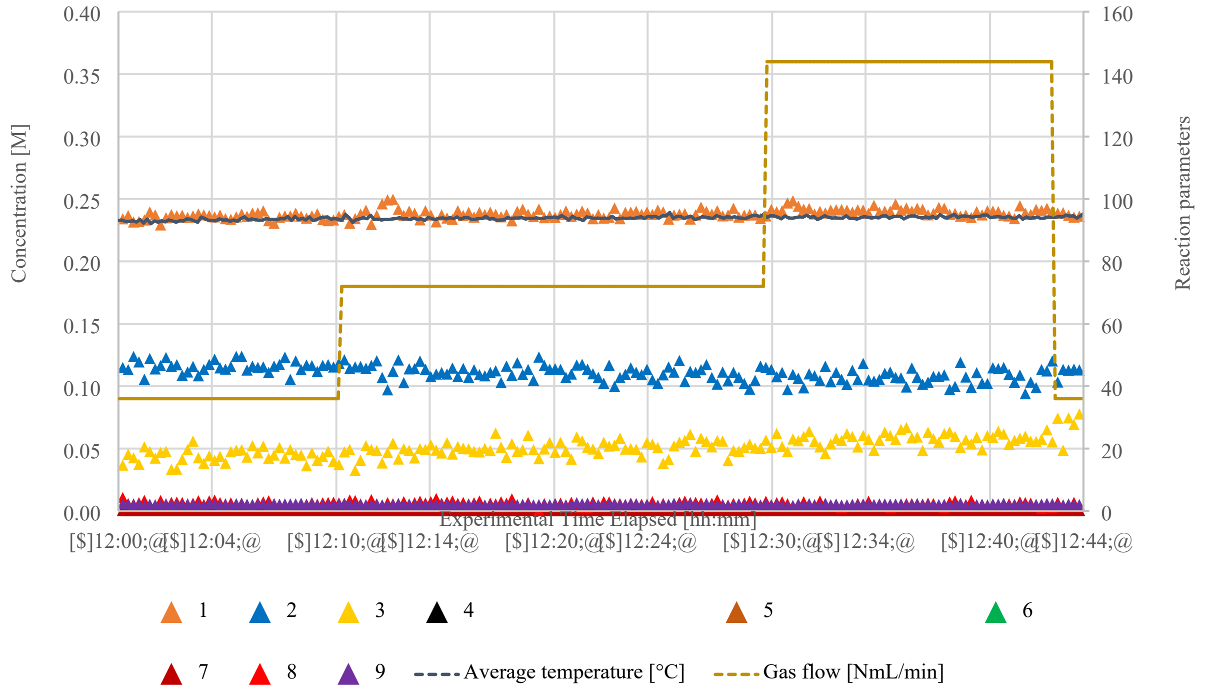

Figure S26. Reaction profile for *Experiment 10*.

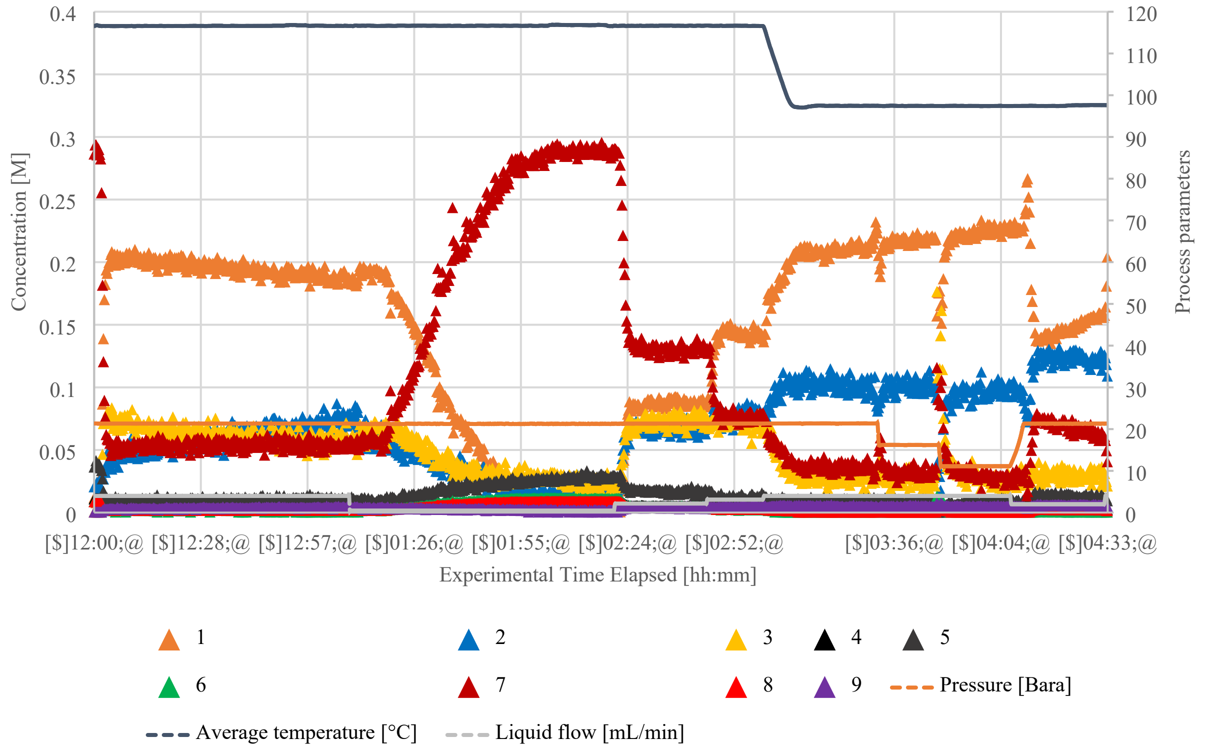

Figure S27. Reaction profile for *Experiment 11*.

The deactivation of the catalyst at low temperature can be stopped either using higher temperatures or by the addition of water. This second approach was used in Experiment 12, which confirmed the effectiveness of water addition in preventing catalyst deactivation.

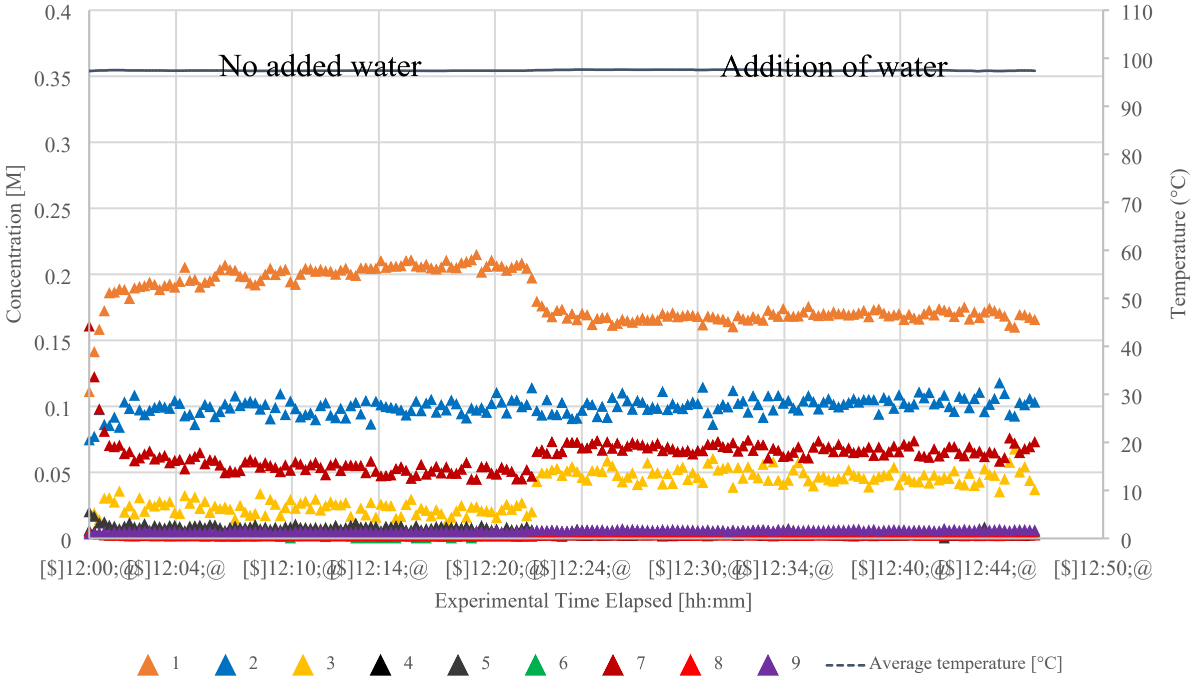

Figure S28. Reaction profile for *Experiment 12.*

6. Batch-Approximated Kinetic modeling

6.1. Conversion of Experimental Time to Residence Time

For the kinetic analysis of the experimental data using a batch approximation approach, the experimental time, i.e., relative to the start of the experiment (from when the first temperature section was started), was converted into a residence time. The procedure makes use of the following equation.

$$V = \int_{t_0}^{t_m} Q(t) \cdot dt = \int_{t_0}^{t_m} (Q_0 + \alpha \cdot t) \cdot dt$$

Where V is the volume of the reactor, Q(t) is the flow ramp over time, calculated from a starting point (t_0) to a measuring point (t_m), Q_0 is the starting flow at steady state and α is the flow ramp. The approach used in this work follows the following principles:

- To simplify the calculation, at the start of the ramp t_0 is equal to 0, regardless of the experimental time.
- The equation is applied only on the ramps and does not consider the steady states. Therefore, for each temperature it is applied twice, once for the ramp from low to high flow and one for the ramp from high to low flow.
- To synchronize the IR data to their actual residence time, the equation above was solved for t_0. To each value of t_m it was thus possible to assign a value of t_o and therefore a residence time, calculated as the difference from the two values.
- For the points whose measured time is within the time range of the ramp, the solution of the above equation for t_0 gives the following equations:

$$t_0 = \frac{Q_0 - \sqrt{Q_0^2 + 2 \cdot \alpha \cdot \left(\frac{\alpha}{2} \cdot t_m^2 + Q_0 \cdot t_m - V \right)}}{(-\alpha)}$$

With α<0 for the ramp from high to low flow and α>0 for the one from low to high flow.

- As the points injected at the end of the ramps will experience a certain time at constant flow, the equation above must be modified to include these sections. The equation can be modified in the following way.

$$V = \int_{t_0}^{30} (Q_0 + \alpha \cdot t) \cdot dt + \int_{30}^{t_m} Q_m \cdot dt$$

Where Q_m is either equal to 0.5 mL/min if the ramp is from high to low flow (with Q_0 equal to 4 mL/min) or to 4 mL/min (with Q_0 equal to 0.5 mL/min). The solutions for the two ramps (ramp UP and ramp DOWN) are therefore.

$$t_0^{DOWN} = \frac{4 - \sqrt{16 + 2 \cdot \alpha \cdot (450 \cdot \alpha + 0.5 \cdot t_m + 105 - V)}}{(-\alpha)}$$

$$t_0^{UP} = \frac{0.5 - \sqrt{0.25 + 2 \cdot \alpha \cdot (450 \cdot \alpha + 4 \cdot t_m - 105 - V)}}{(-\alpha)}$$

Where the values of the Q_0 and Q_m have already been substituted.

- Particular care must be taken in determining the transition from a full ramp injection point (i.e., a sample which, upon injection, is subjected to a full ramp profile) and mixed ramp injection points (i.e., samples which are partially subjected to a ramp and partially to a steady state). The transition between the two can be computed by calculating the injection time of the samples whose measured value occurs at the end of the ramp (t_m equal to 30 min). For the ramp from low to high (ramp up) flow this time is equal to 24.41 min, whereas for high to low flow (ramp down) it is equal to 23.12 min.
- There is a dead volume between the end of the reactor and the points at which FT-IR samples are measured. This volume is 2.8 mL. The residence time, calculated as difference between t_0 and t_m has to be corrected accordingly.

The profiles of the residence times for the two ramps are shown in **Figure S*29***.

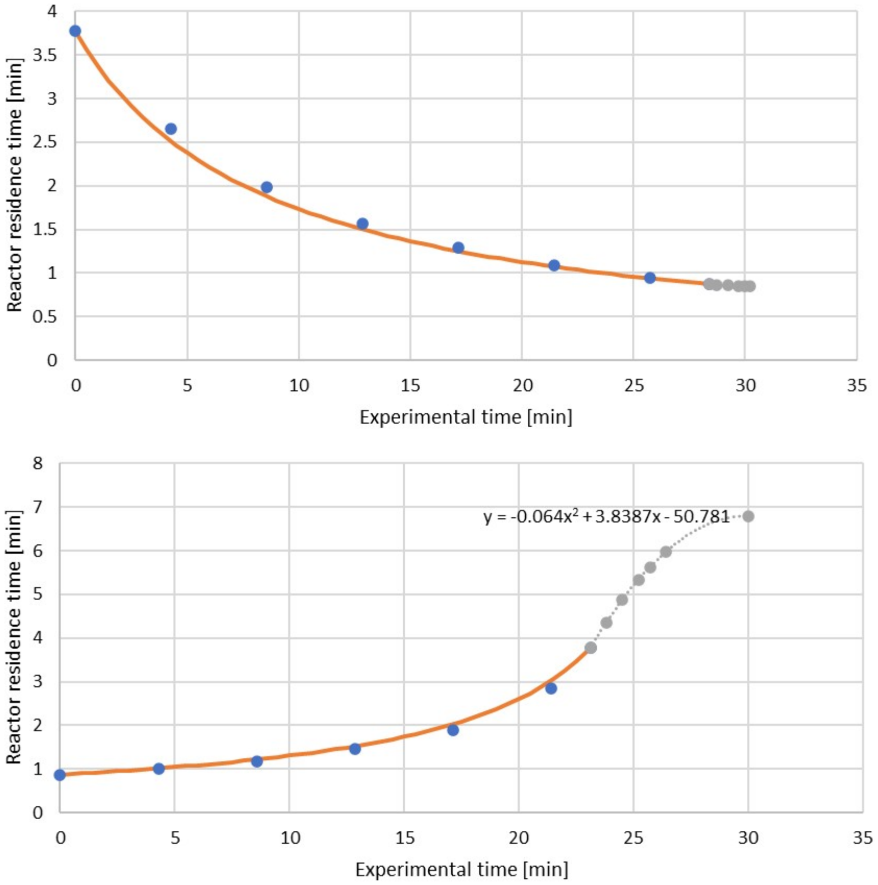

Figure S29. Plots showing the conversion of experimental time to residence time for the specified sequence of flow rate ramps.

As it can be seen a ramp down gives a wider range of residence times than a ramp up. This is because during a ramp down an injected sample spends more time at shorter residence time, whereas for a ramp up the opposite occurs. This also may imply that for a ramp up there is a better solution changeover in the dead volume and this may give small discrepancies in the results with large dead volumes especially when low flows are used.

6.2. Kinetic Modeling Using MATLAB

For the determination of the reaction kinetics the code was implemented with the MATLAB functions *fmincon* for function minimization and the ode suite *ode45* for the resolution of the system of ordinary differential equations. The determination of the error of the kinetic constants was done using the function *nlparci* with the implementation of the covariance matrix obtained using the *nlinfit* function. The function to minimize was the normalized base 2 norm.

Kinetic modeling was performed assuming different kinetic network options and evaluating for each of them the Akaike Information Criterion (AIC),[2] defined as

$$AIC = n \cdot \ln\left(\frac{SSE}{n}\right) + 2 \cdot k$$

Where n is the number of observations, SSE is the sum square of error of the model and k the number of parameters.

The model having the lowest value was assumed to be the most suitable. All the reaction kinetics were assumed to be first order. Different reaction networks were evaluated: for palladium two models (1 and 2) were considered; for platinum and ruthenium model 3 to 10 were analyzed. The models proposed and the AIC values are reported below. For the selected model the kinetic constants are listed with the associated error. Finally, the Arrhenius parameters (activation energy and pre-exponential factor) for the major reaction pathways are reported.

6.2.1. Pd/Al_2O_3

Catalyst: Pd/Al_2O_3

<table>
<tr><th>Model 1</th><th>Model 2</th></tr>
<tr><td>
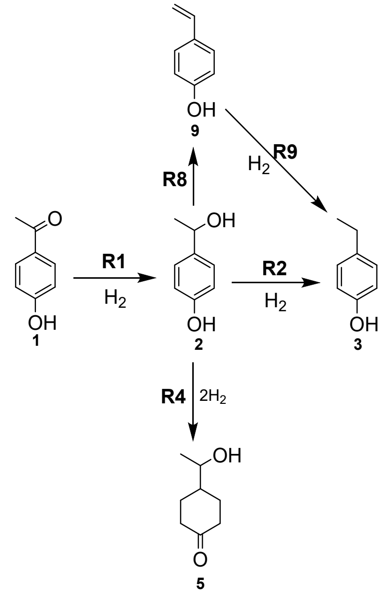

</td><td>
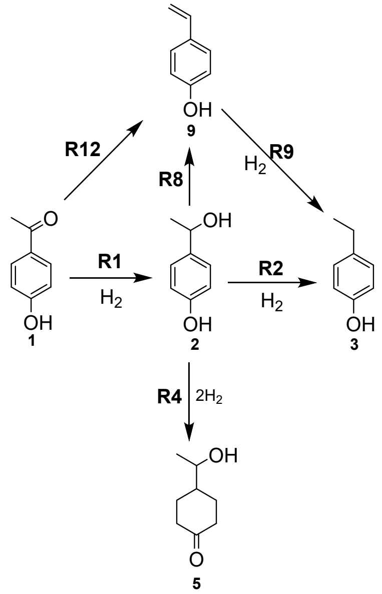

</td></tr>
</table>

	AIC at 100°C
Model 1	-4.642E+03
Model 2	-4.640E+03

Model 1 was selected. The kinetic constants calculated at 80, 100, 120 and 140 °C and the Arrhenius parameters (calculated between 100 and 140 °C) are listed below. Only those constants statistically above 0 were considered for the evaluation of Arrhenius parameters.

Temperature (°C)		**k1 (1/(M s))**	**k2 (1/(M s))**	**k4 (1/(M s))**	**k8 (1/(M s))**	**k9 (1/(M s))**
80	**Value**	0.00070	0.00000	0.00000	0.00346	0.11558
	95% CI	0.00001	0.02622	0.00008	0.02623	0.86849
100	**Value**	0.00257	0.00838	0.00016	0.00036	0.00402
	95% CI	0.00004	0.00111	0.00011	0.00111	0.01905
120	**Value**	0.00586	0.02400	0.00022	0.00028	0.00135
	95% CI	0.00015	0.00145	0.00027	0.00129	0.01004
140	**Value**	0.01520	0.10762	0.00131	0.00027	0.00000
	95% CI	0.00044	0.00920	0.00097	0.00241	0.00511

	E_a (kJ/mol)	**95% CI (kJ/mol)**	**A**	**95% CI (low)**	**95% CI (high)**
Reaction 1	57	2	2.9E+05	-1.5E+05	3.1E+05
Reaction 2	82	1	2.7E+09	-7.5E+08	1.0E+09

The following reaction profiles were fitted.

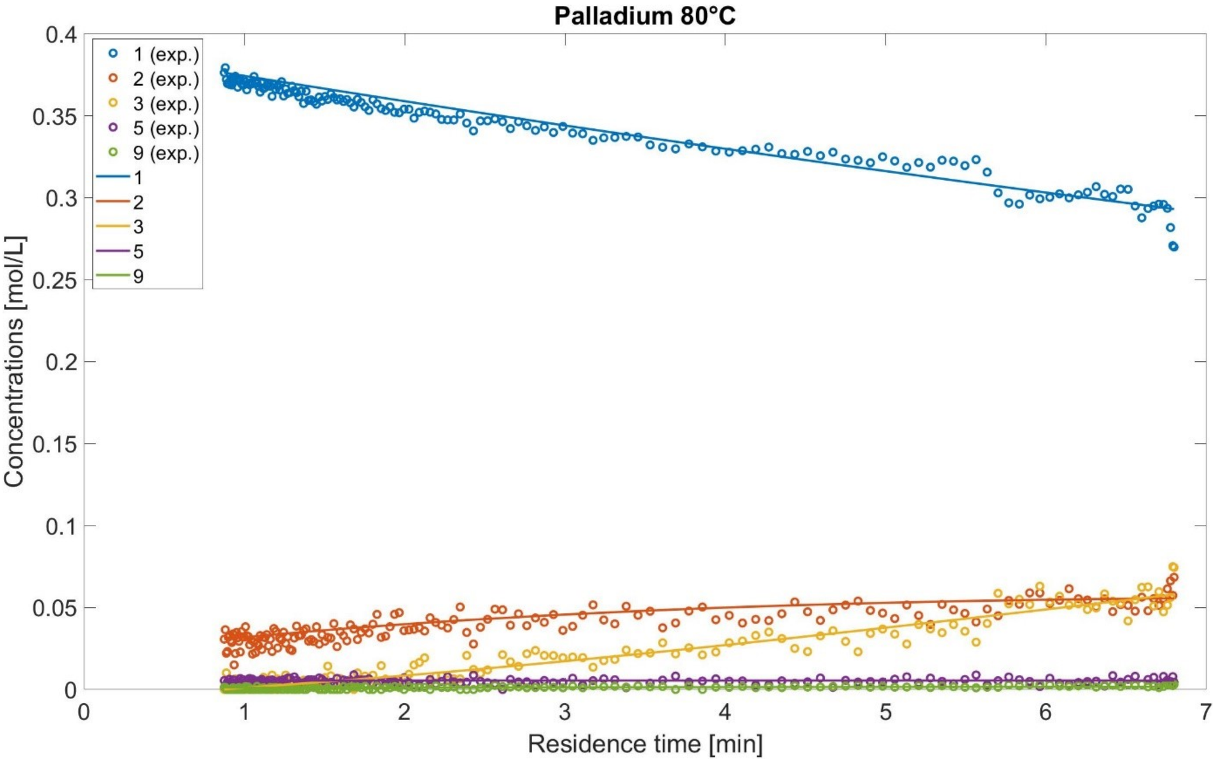

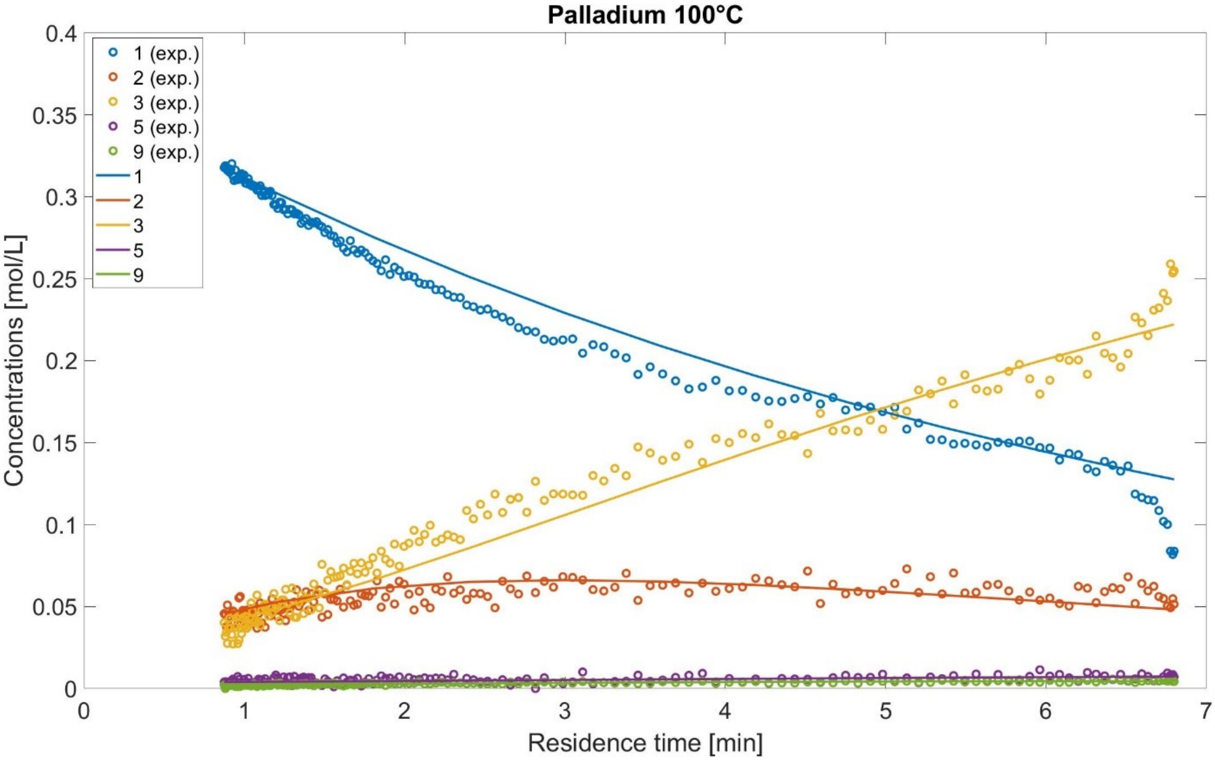

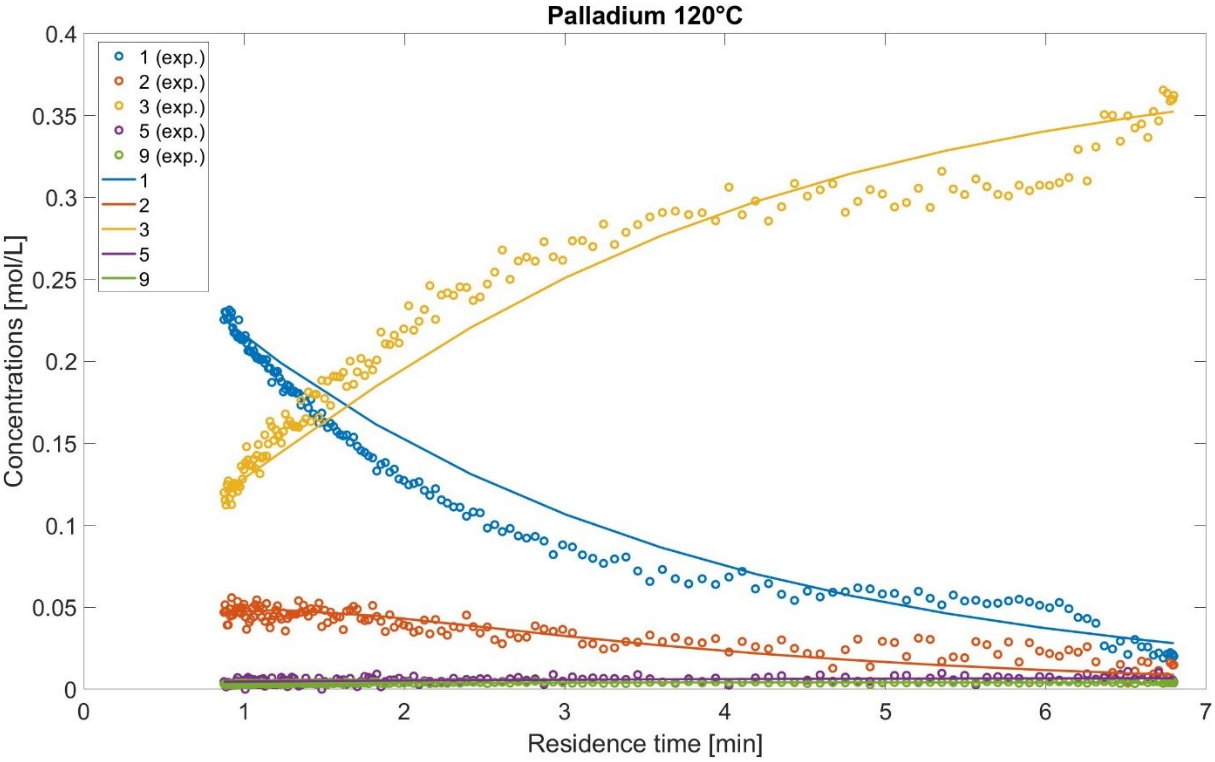
Palladium 120°C
Concentrations [mol/L]
Residence time [min]
0
0.05
0.1
0.15
0.2
0.25
0.3
0.35
0.4
0
1
2
3
4
5
6
7
1 (exp.)
2 (exp.)
3 (exp.)
5 (exp.)
9 (exp.)
1
2
3
5
9

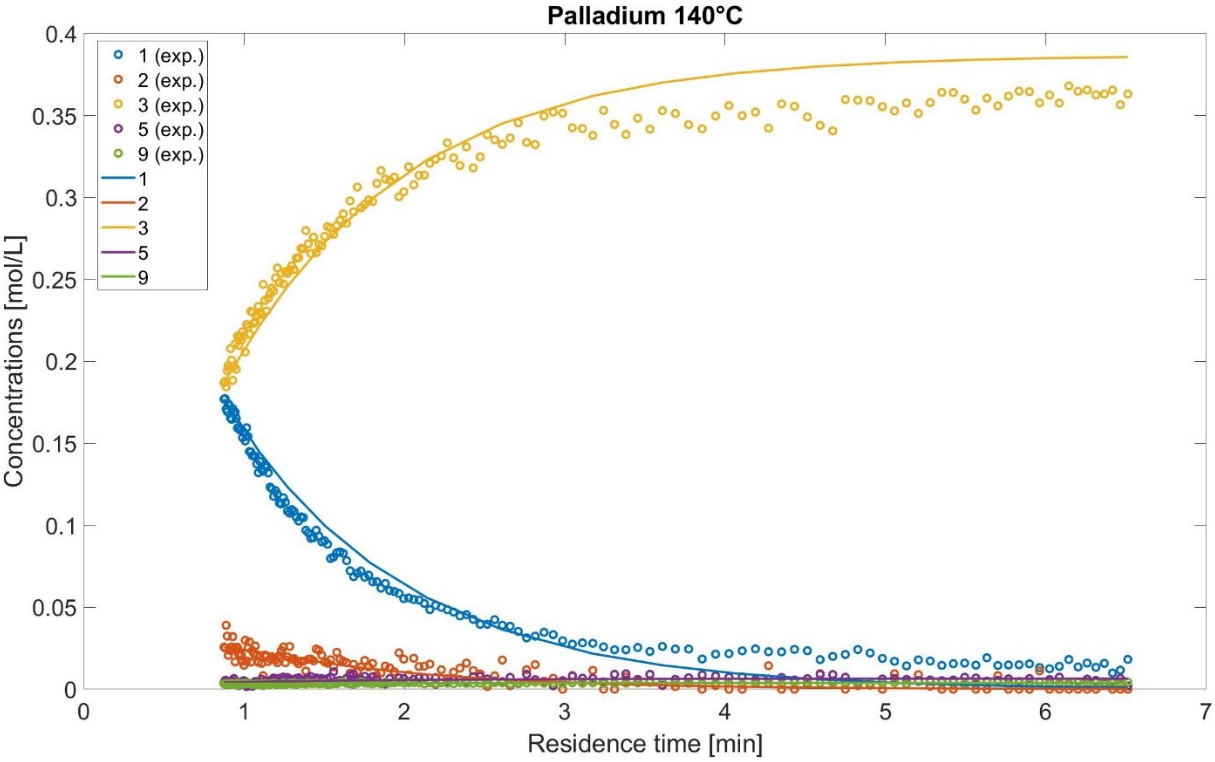
Palladium 140°C
Concentrations [mol/L]
Residence time [min]
0
0.05
0.1
0.15
0.2
0.25
0.3
0.35
0.4
0
1
2
3
4
5
6
7
1 (exp.)
2 (exp.)
3 (exp.)
5 (exp.)
9 (exp.)
1
2
3
5
9

6.2.2. Ru/Al_2O_3

Model 3	**Model 4**
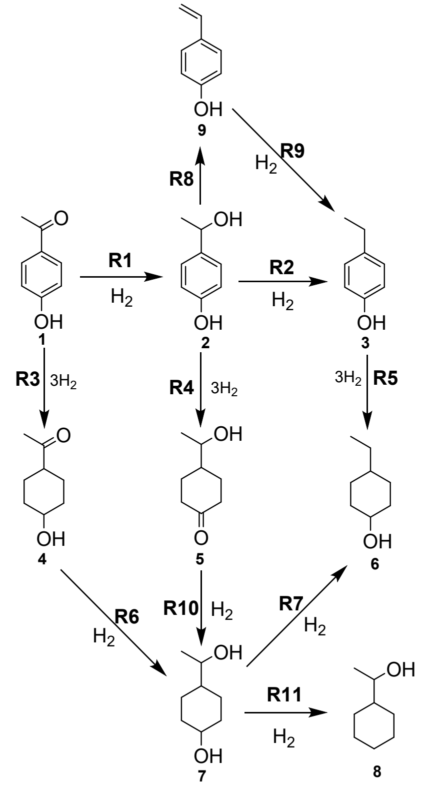	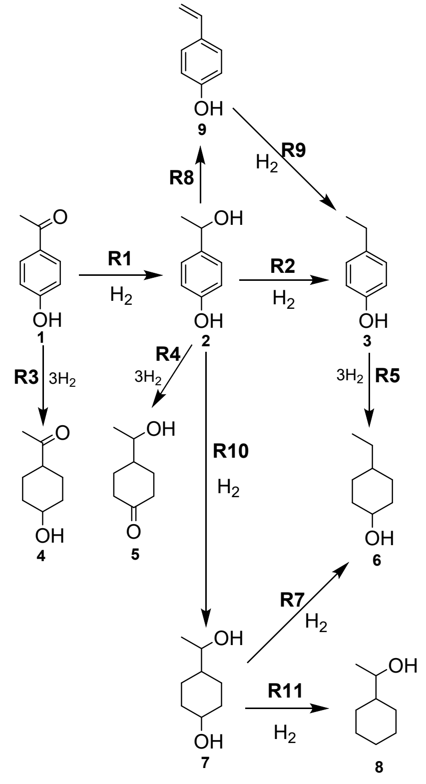
Model 5	**Model 6**
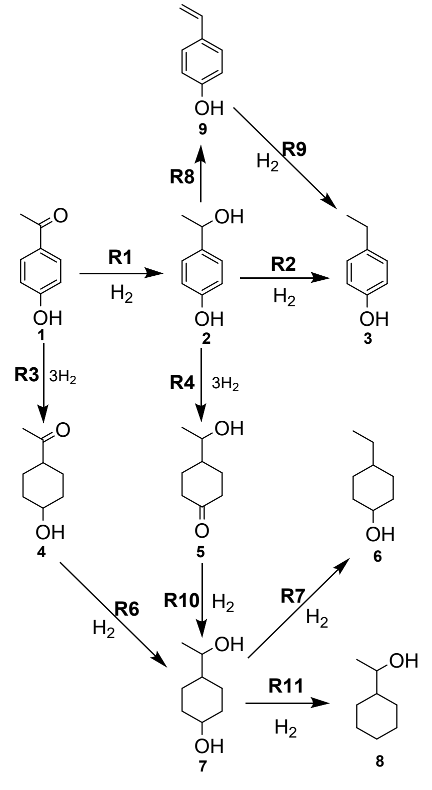	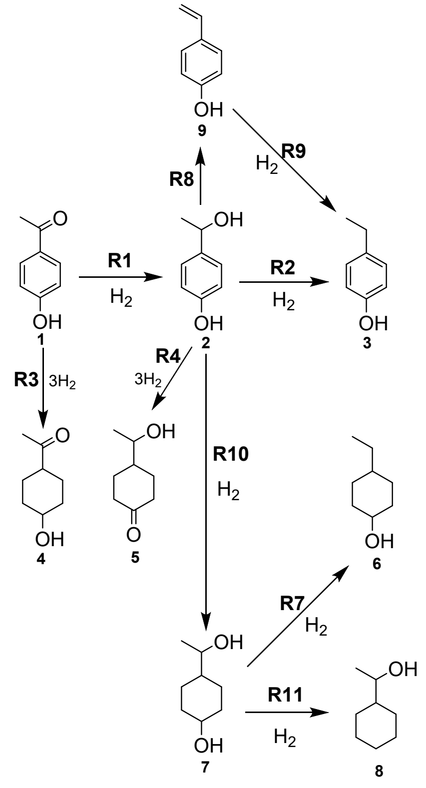

Model 7	**Model 8**
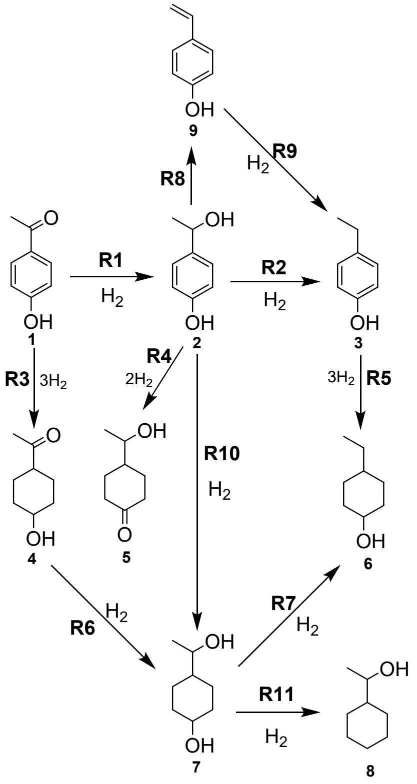	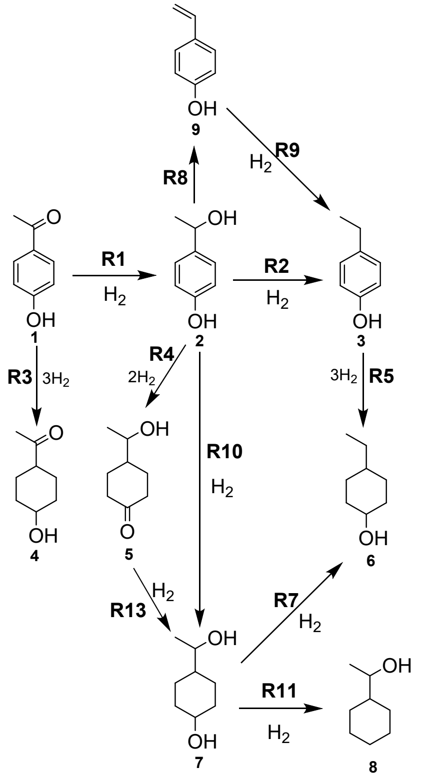
Model 9	**Model 10**
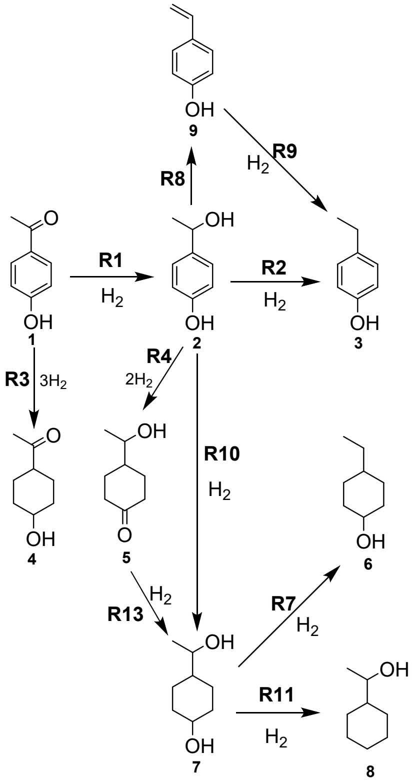	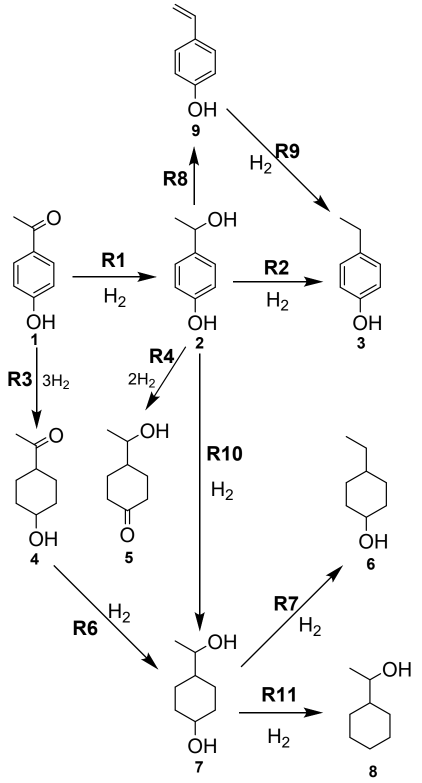

	AIC at 100°C
Model 3	-8.485E+03
Model 4	-8.610E+03
Model 5	-8.484E+03
Model 6	-8.610E+03
Model 7	-8.610E+03
Model 8	-8.613E+03
Model 9	-8.613E+03
Model 10	-8.608E+03

Model 8 was selected as more complete than model 9, although the two models yielded similar results.

Temperature (°C)		**k1 (1/(M s))**	**k2 (1/(M s))**	**k3 (1/(M s))**	**k4 (1/(M s))**	**k5 (1/(M s))**	**k7 (1/(M s))**	**k8 (1/(M s))**	**k9 (1/(M s))**	**k10 (1/(M s))**	**k11 (1/(M s))**	**k13 (1/(M s))**
80	**Value**	0.00104	0.00000	0.00002	0.00109	0.00036	0.00007	0.00042	0.00782	0.00246	0.00016	0.00843
	95% CI	0.00001	0.00226	0.00001	0.00111	0.00203	0.00064	0.00225	0.05487	0.00103	0.00017	0.01249
100	**Value**	0.00184	0.00031	0.00005	0.00085	0.00029	0.00006	0.00064	0.01150	0.00513	0.00019	0.00251
	95% CI	0.00002	0.00246	0.00001	0.00035	0.00164	0.00049	0.00251	0.05075	0.00040	0.00007	0.00355
120	**Value**	0.00255	0.00196	0.00007	0.00133	0.00046	0.00000	0.00040	0.00561	0.00793	0.00019	0.00311
	95% CI	0.00005	0.00184	0.00003	0.00063	0.00120	0.00048	0.00202	0.03455	0.00062	0.00009	0.00398

	E_a (kJ/mol)	**95% CI (kJ/mol)**	**A**	**95% CI (low)**	**95% CI (high)**
Reaction 1	26	3	8.6	-5.7	17.3
Reaction 10	34	4	320.9	-232.1	838.2

The following reaction profile were fitted.

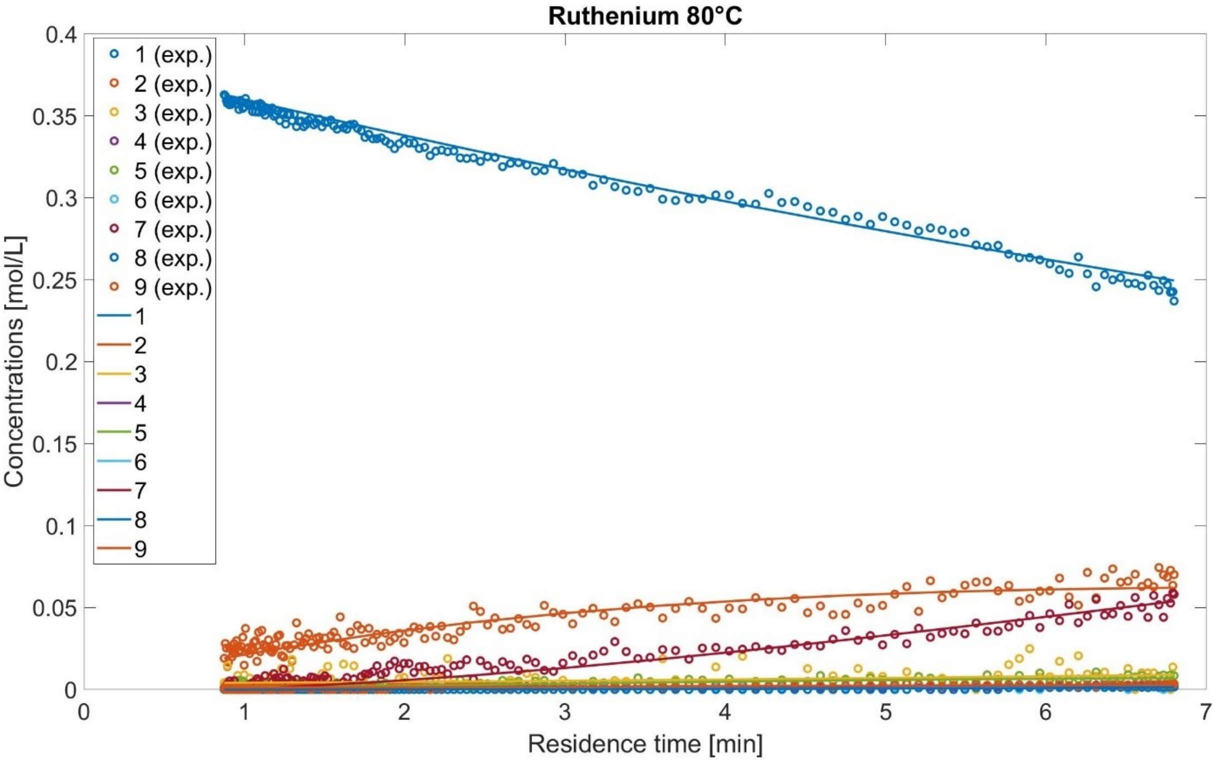

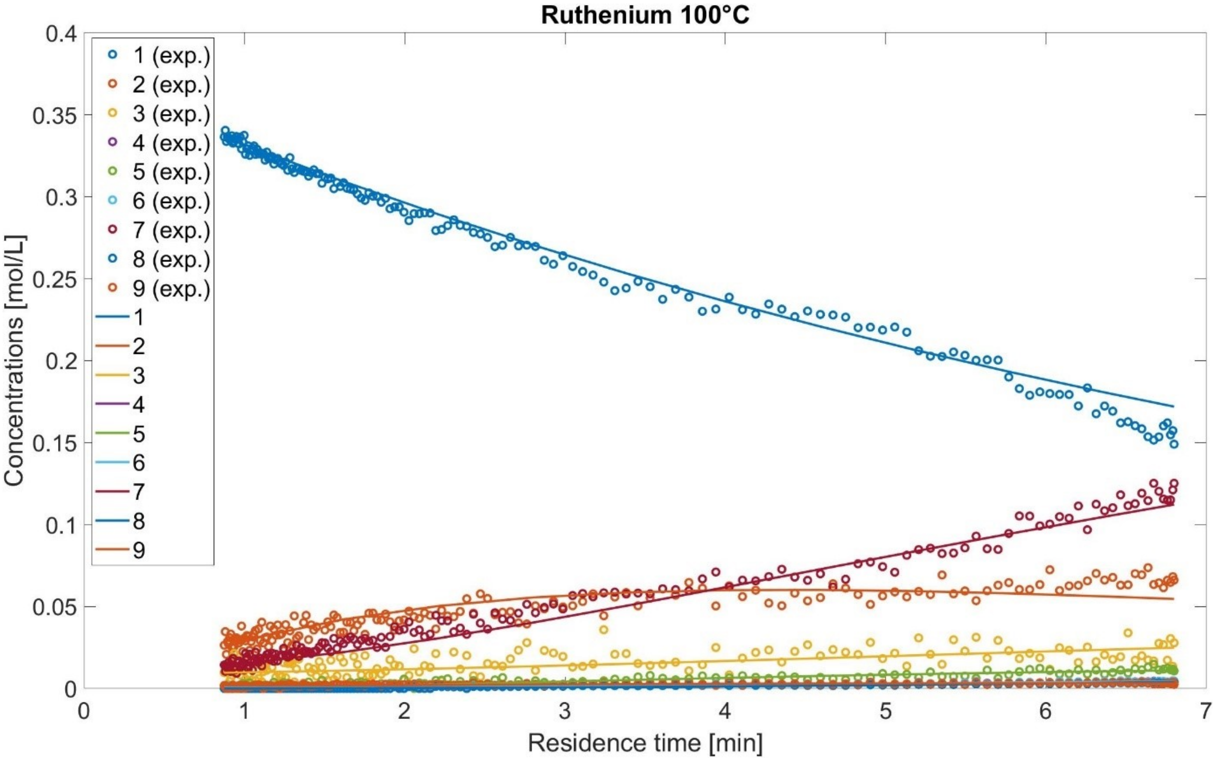

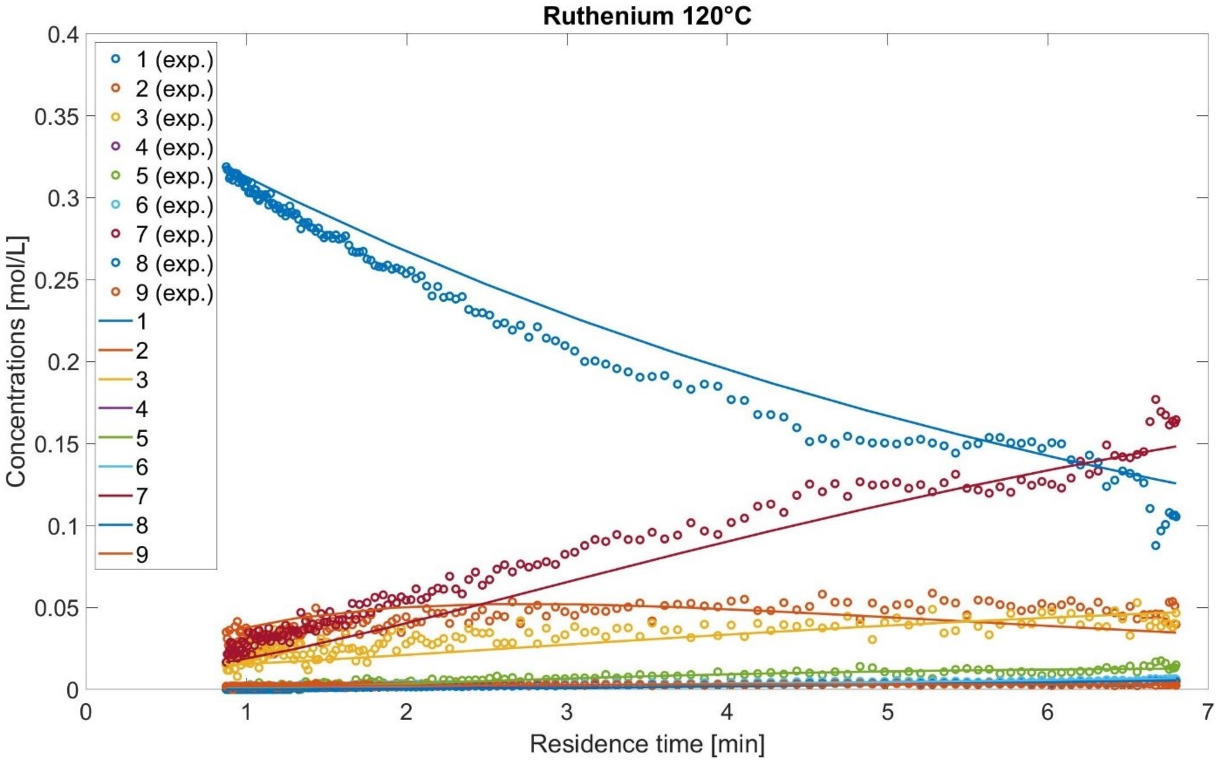
Ruthenium 120°C
Concentrations [mol/L]
Residence time [min]
0.4
0.35
0.3
0.25
0.2
0.15
0.1
0.05
0
0
1
2
3
4
5
6
7
1 (exp.)
2 (exp.)
3 (exp.)
4 (exp.)
5 (exp.)
6 (exp.)
7 (exp.)
8 (exp.)
9 (exp.)
1
2
3
4
5
6
7
8
9

6.2.3. Pt/Al_2O_3

See model definition above, as for Ru/Al_2O_3. Model 4 was selected.

	AIC at 100°C
Model 3	-7.668E+03
Model 4	-8.511E+03
Model 5	-7.628E+03
Model 6	-8.395E+03
Model 7	-8.459E+03
Model 8	-8.511E+03
Model 9	n/a
Model 10	-8.393E+03

Temperature (°C)		**k1 (1/(M s))**	**k2 (1/(M s))**	**k3 (1/(M s))**	**k4 (1/(M s))**	**k5 (1/(M s))**	**k7 (1/(M s))**	**k8 (1/(M s))**	**k9 (1/(M s))**	**k10 (1/(M s))**	**k11 (1/(M s))**
60	**Value**	0.00205	0.00011	0.00004	0.00018	0.00188	0.00000	0.00038	0.00630	0.00253	0.00019
	95% CI	0.00002	0.00073	0.00001	0.00004	0.00394	0.00042	0.00079	0.01898	0.00016	0.00009
80	**Value**	0.00466	0.00000	0.00012	0.00056	0.00131	0.00000	0.00029	0.00517	0.00577	0.00017
	95% CI	0.00005	0.00062	0.00003	0.00005	0.00133	0.00016	0.00059	0.01340	0.00019	0.00004
100	**Value**	0.00899	0.00099	0.00032	0.00110	0.00165	0.00000	0.00008	0.00393	0.01386	0.00011
	95% CI	0.00015	0.00068	0.00006	0.00009	0.00081	0.00008	0.00075	0.01330	0.00027	0.00003

	E_a (kJ/mol)	**95% CI (kJ/mol)**	**A**	**95% CI (low)**	**95% CI (high)**
Reaction 1	39	1	2.4E+03	-9.4E+02	1.6E+03
Reaction 4	47	6	4.7E+03	-4.0E+03	2.7E+04
Reaction 10	44	2	2.2E+04	-1.1E+04	2.2E+04

The following reaction profiles were recorded.

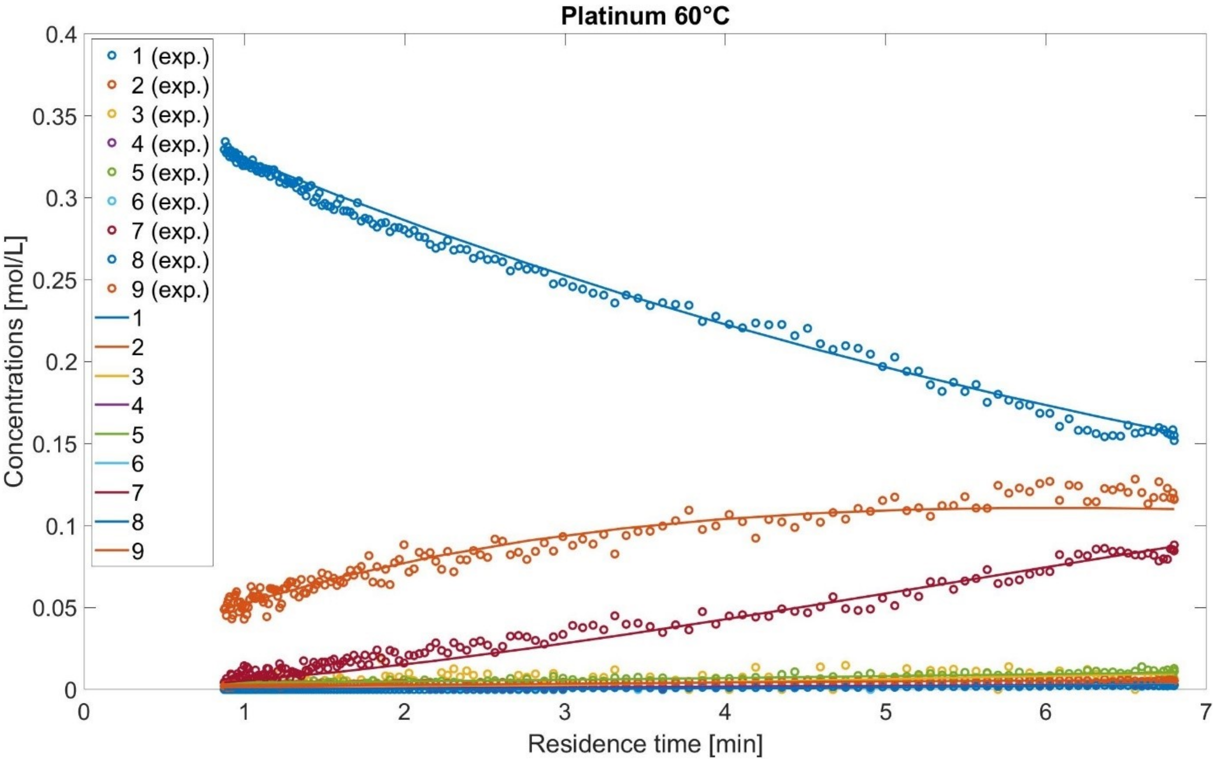

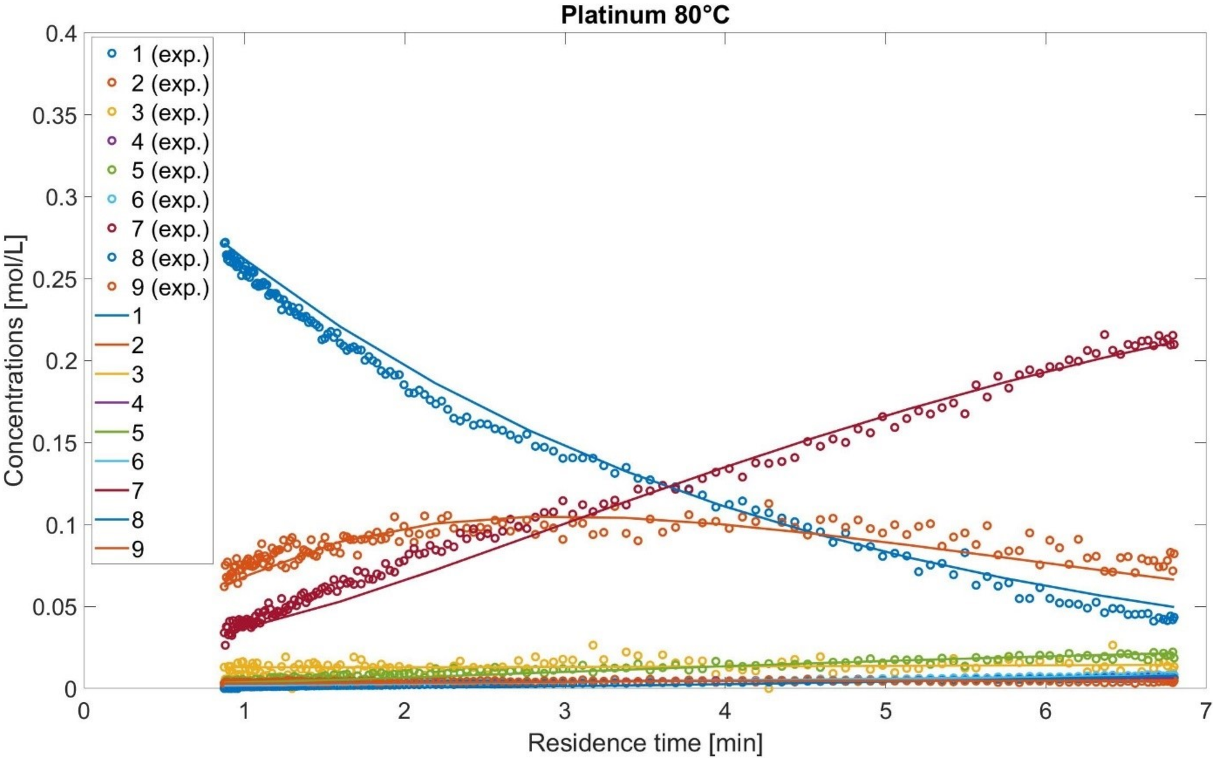

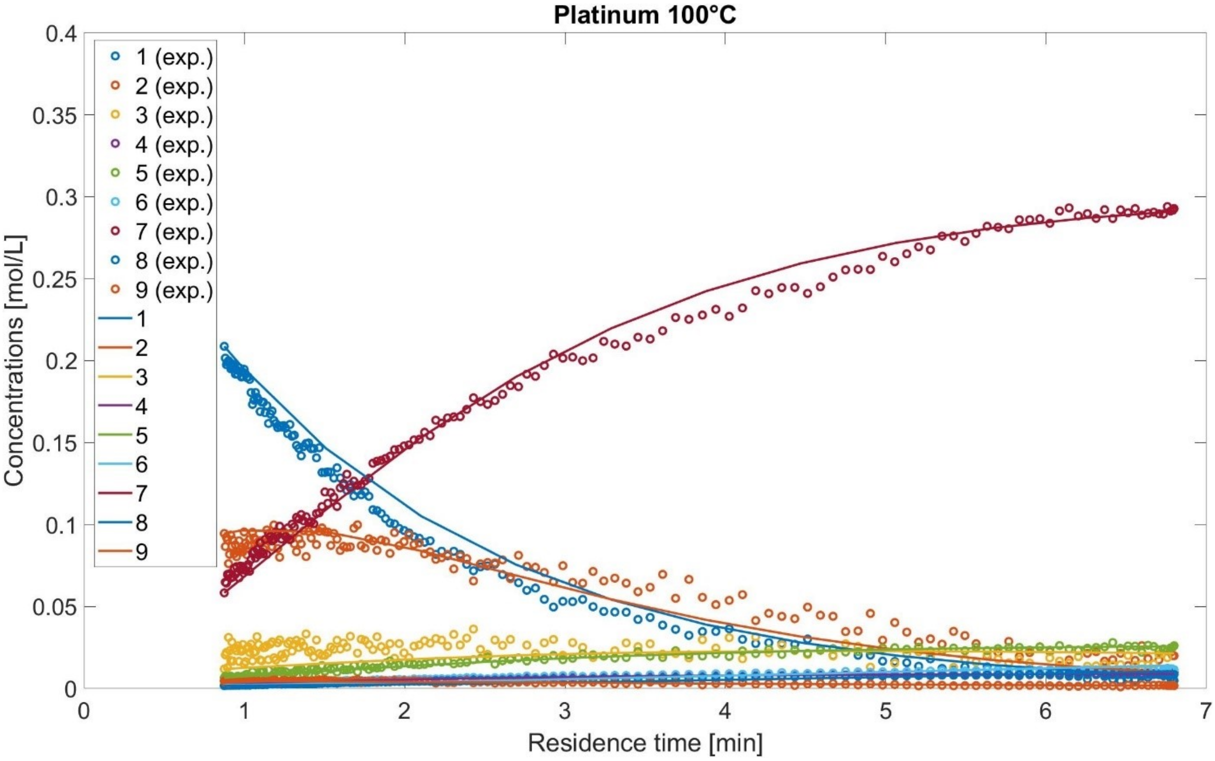
Platinum 100°C
0.4
0.35
0.3
0.25
0.2
0.15
0.1
0.05
0
Concentrations [mol/L]
0
1
2
3
4
5
6
7
Residence time [min]
1 (exp.)
2 (exp.)
3 (exp.)
4 (exp.)
5 (exp.)
6 (exp.)
7 (exp.)
8 (exp.)
9 (exp.)
1
2
3
4
5
6
7
8
9

7. Plug Flow Reactor Kinetic Modeling

7.1. Plug Flow Reactor Model

The basis of the model is an isothermal plug flow reactor model.[3] The key modeling assumptions are:

i) A plug flow reactor is assumed, i.e., diffusion is negligible.

ii) The reactor is isothermal, i.e., the temperature dynamics are neglected due to the low reactor volume. The reactor temperature is kept constant via a heat exchanger.

iii) The catalyst surface dynamics are neglected. It is assumed that the hydrogen is adsorbed onto the catalyst surface at a faster rate than other reactions occur. This assumption is a simplification to avoid overparameterization of the model, because it is not practicable to measure (directly or indirectly) the hydrogen concentration adsorbed to the catalyst surface.

The aforementioned assumptions and simplifications still allow to accurately describe the reaction kinetics. The concentration of the species C_j for $j = 1, \ldots, n$ depends on space z and time t. The concentrations are summarized in the vector

$$C(z,t) = \begin{bmatrix} C_1(z,t) \\ C_2(z,t) \\ \vdots \\ C_n(z,t) \end{bmatrix} \tag{1}$$

with n as the number of considered species. The plug flow reactor model for the concentration C_j of a single species j is then given by

$$\frac{\partial C_j(z,t)}{\partial t} = -q(t)\frac{\partial C_j(z,t)}{\partial z} + b_j^T r(t,z,T) \tag{2}$$

Here, $q(t)$ is the flowrate and $T(t)$ is the reactor temperature, controlled by the heat exchanger. This equation is defined for time $t \geq 0$ and on the spatial domain $z_1 \in [0,\ V_r]$ with V_r as the reactor volume.

Note that in this formulation, it is assumed that the reactor cross section is normalized to 1, which results in a (modeled) reactor length of V_r. This approach was chosen to simplify the reactor coordinate, due to the differences in reactor geometry in different sections (e.g., different tubing diameters).

The boundary and initial conditions are given by

$$C_j(0,t) = C_{j,\,in}(t) \tag{3}$$

and

$$C_j(z,0) = C_{j,0} \tag{4}$$

respectively. Here, $C_{j,\,in}(t)$ is the inlet concentration of species *j*.

The term $b_j^T r(t,z,T)$ models the reaction network from manuscript Figure 2.

The column vector

$$r(t,z,T) = \begin{bmatrix} r_1(t,z,T) \\ r_2(t,z,T) \\ \vdots \\ r_m(t,z,T) \end{bmatrix} \tag{5}$$

models the reaction rates for the $m = 10$ reactions. All reactions are modeled as a first order reaction following the Arrhenius law, i.e.,

$$r(t,z,T) = k_{i,0} e^{-\frac{Ea,i}{RT}} C_l(z,t) \tag{6}$$

Here, the pre-exponential factor is given by $k_{i,0}$ and $E_{a,i}$ denotes the activation energy for reaction *i*. The species involved in the reaction are donated by C_l and can be obtained from the concentration vector via

$$C_l = e_l^T C \tag{7}$$

where e_l is the l-th Euclidian basis vector. The row vector b_j^T models the mass balance for species j. As an example, take the starting material **1**. It reacts to form **2** (via the reaction path R1) or **4** (via the reaction path R3). This gives

$$r(t,z,T) = [-1 \quad 0 \; -1 \quad 0 \quad 0 \quad 0 \quad 0 \quad 0 \quad 0 \quad 0 \quad 0] \tag{8}$$

Because there is an additional dead volume present after the reactor (leading to the FTIR and UHPLC analytics), a second model for this inert section is added. It is given by

$$\frac{\partial C_j(z,t)}{\partial t} = -q(t)\frac{\partial C_j(z,t)}{\partial z} \tag{9}$$

for $j = 1,\ldots, n$. This model is defined on the spatial domain $z \in [V_r, V_r + V_i]$, where V_i is the inert volume. Both domains are linked via the interface conditions

$$\lim_{z\to V_r^-} C_j(z,t) = \lim_{z\to V_r^+} C_j(z,t), j = 1,\ldots, n \tag{10}$$

Note: due to the chosen formulation, not only the species concentration but also the flow rate is continuous at the interface between the compartments.

7.1.1. Model Implementation

The model was implemented in Julia using the *MethodOfLines.jl* toolkit. This toolkit allows to formulate PDE models in a high-level programming language. Space discretization via the method of lines (MOL) approach [4] was performed via the toolkit in a straightforward manner. The resulting ODE model was then simulated with the help of the Julia packages *ModelingToolkit.jl* [5] and *OrdinaryDiffEq.jl*. The Julia environment has several advantages compared to other (e.g., Matlab or Python-based) simulation frameworks. The biggest advantage is the high performance of the provided ODE solvers.[6] This allows fast parameter identification and optimization of the operating conditions using a complex simulation model.

7.2. Parameter Identification

The concentrations of the considered species at the reactor outlet were obtained from experimental FTIR measurements. For identification of the reaction kinetics, the model outputs were fitted to the experimental data using a quadratic cost function for the error

$$e(t) = C\left(V_r + V_i, t\right) - C_m\left(V_r + V_i, t\right) \tag{11}$$

where $C_m(V_r + V_i, t)$ is the outlet concentration measured at time t. This results in

$$J = \sum_{k=0}^{N} e^{\top}\left(t_k\right) diag(w) e\left(t_k\right) \tag{12}$$

for the optimization criterion. Here, t_k with $, k = 0, \ldots, N$ are the measurement time instants and $w \in R^n$ is a tuning parameter containing weights for different species. This allows a higher weighting to be placed on a specific species' outlet concentration during the identification procedure. The parameter identification was conducted using *DiffEqParamEstim.jl* and *Optimization.jl* packages in Julia. The latter provided support for different (nonlinear) optimization algorithms. From a wide variety of different solvents, the BOBYQA solver[7] from the *NLopt* toolbox was selected, since it rapidly provided results with good accuracy.

Parameterization for all three catalysts is shown below.

7.2.1. Pd/Al_2O_3

Parameters were identified using data from experiment 1 (see Section 5 for details).

Table S8. Reaction parameters found for the Pd/Al_2O_3 catalyst model.

Reaction	Pre exponential factor A (*E4)	Activation Energy Ea (kJ/mol)
R1	9.8646	49.3021
R2	7.9802	50.7377

A plot of predicted vs measured concentrations for this experiment can be found in the main manuscript (Figure 5)

7.2.2. Ru/Al_2O_3

Parameters were identified using data from experiment 4 (see Section 5 for details).

Table S9. Reaction parameters found for the Ru/Al_2O_3 catalyst model.

Reaction	Pre exponential factor A (*E4)	Activation Energy Ea (kJ/mol)
R1	0.045123	38.2606
R4	12.4551	57.1369
R10	11.1789	51.8724

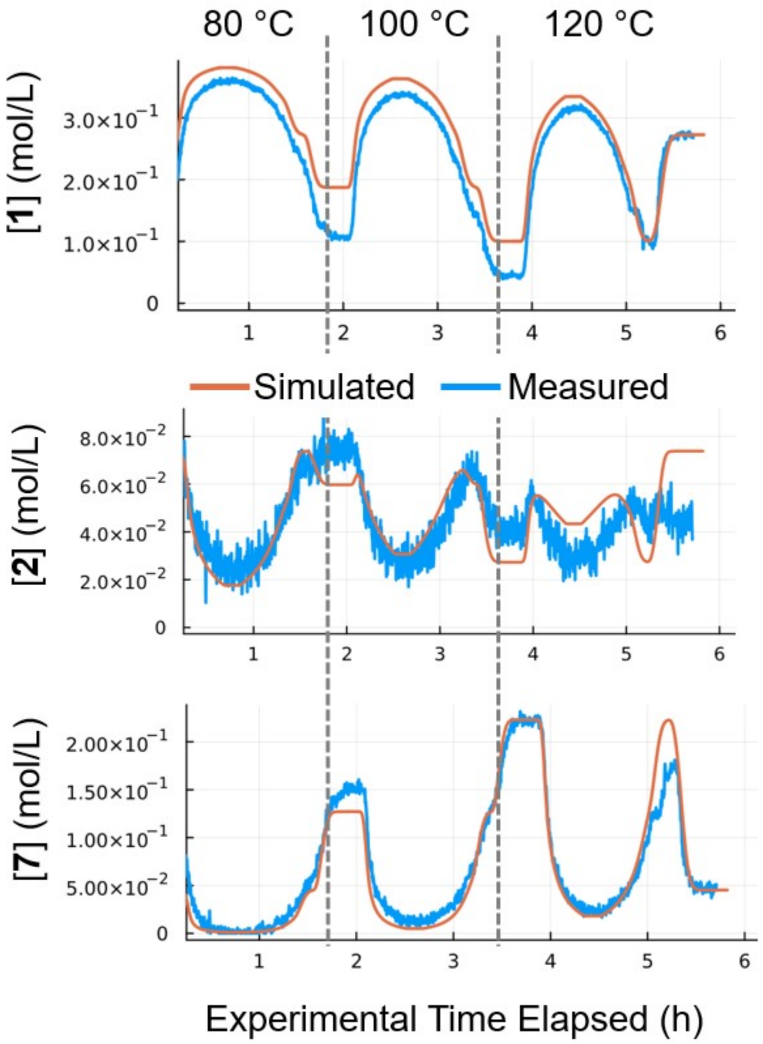

Figure S30. Predicted vs measured concentrations, using the parameterized model, for experiment 4.

7.2.3. Pt/Al_2O_3

Parameters were identified using data from experiment 6 (see Section 5 for details).

Table S10. Reaction parameters found for the Pt/Al_2O_3 catalyst model.

Reaction	Pre exponential factor A (*E4)	Activation Energy Ea (kJ/mol)
R1	10.597	48.44
R4	9.629	94.90
R10	12.248	48.01

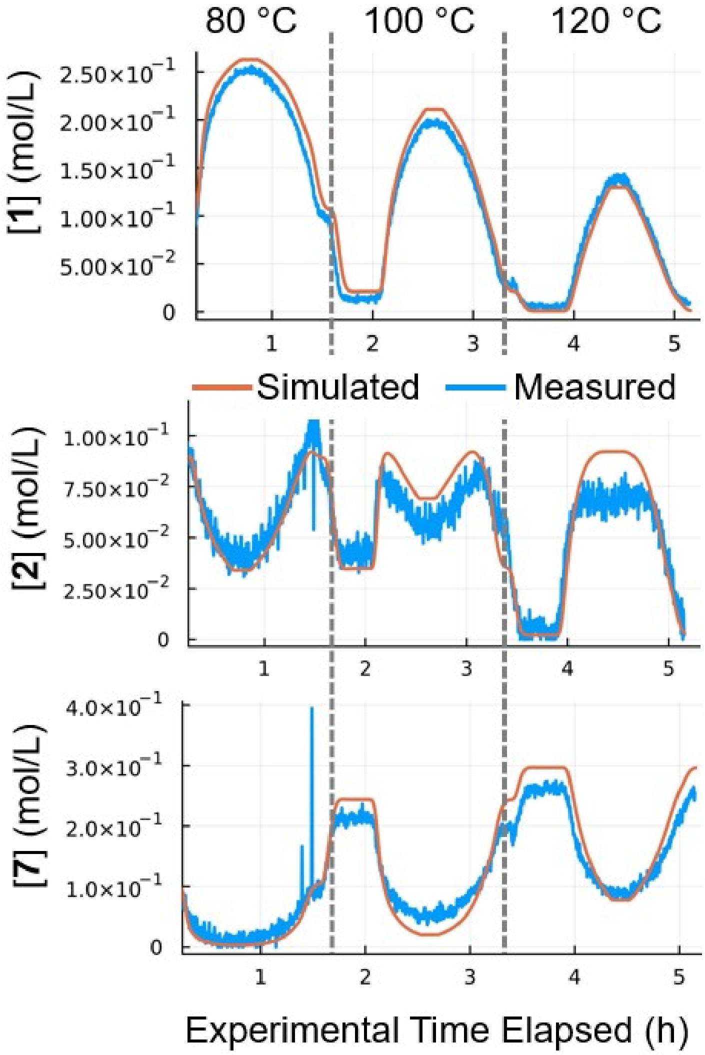

Figure S31. Predicted vs measured concentrations, using the parameterized model, for experiment 6.

7.3. Optimal Operating Point Definition

In order to obtain optimal steady state operating conditions for the reactor, i.e., optimal flowrate and temperature, a multi-objective optimization was performed based on the simulation model. For this, $q(t) = q_0$ and $T(t) = T_0$ were assumed constant and regarded as parameters which should be optimized. For this, the parameter vector $p = [q_0\, T_0]^\top \in P$, with P as the allowed parameter space, was introduced. In this formulation, the steady state output concentrations are only a function of the parameter vector p.

One possibility for a cost function could be to maximize selectivity and productivity with respect to desired species C_d. This approach is described in detail in the following. The concentration of **1** is defined as C_1 with its constant input concentration $C_{1,in}$. Moreover, the concentration of some other species j at the reactor outlet in steady state is denoted by $C_{j,out}^{ss}(p)$. The selectivity with respect to species j can be defined as

$$sel_j(p) = \frac{C_{j,out}^{ss}(p)}{C_{1,in} - C_{j,out}^{ss}(p)} \tag{13}$$

The productivity is defined as $prod_j(p) = C_{j,out}^{ss}(p) q_0 = C_{j,out}^{ss}(p) p_1$, which allows the resulting multi-objective problem to be formulated as such:

$$\max_{p \in P} \, [sel_j(p), prod_j(p)] \tag{14}$$

To obtain the steady-state output concentrations, a simulation of the reactor model is performed until steady state is reached. The simulation is very fast in the chosen modeling and simulation framework (a few milliseconds on a standard office PC), which allows the approach to be used within an optimization algorithm. Hence, it is preferred over other methods for computing the steady state. In order to solve the multi-objective optimization problem, the *Metaheuristics.jl* package from Julia was utilized. This package provides support for different single- and multi-objective optimization algorithms, such as NSGA-II, which was used to solve this problem.

8. References

(1) Lebl, R.; Bachmann, S.; Tosatti, P.; Sedelmeier, J.; Püntener, K.; Williams, J. D.; Kappe, C. O. Catalytic Static Mixer-Enabled Hydrogenation of a Key Fenebrutinib Intermediate: Real-Time Analysis for a Stable and Scalable Process. *Org. Process Res. Dev.* **2021**, *25*, 1988–1995.

(2) Akaike, H. Fitting Autoregressive Models for Prediction. *Ann. Inst. Stat. Math.* **1969**, *21*, 243–247.

(3) Pitarch, J. L.; Rakhshan, M.; Mardani, M. M.; Sadeghi, M. S.; de Prada, C. Distributed Nonlinear Control of a Plug-Flow Reactor Under Saturation. *IFAC-PapersOnLine* **2016**, *49*, 87–92.

(4) Schiesser, W. E. Method of Lines PDE Analysis. In *Biomedical Science and Engineering*; John Wiley & Sons, Ltd, 2016.

(5) Ma, Y.; Gowda, S.; Anantharaman, R.; Laughman, C.; Shah, V.; Rackauckas, C. ModelingToolkit: A Composable Graph Transformation System For Equation-Based Modeling. *arXiv* **2021**, arXiv:2103.05244.

(6) Rackauckas, C.; Nie, Q. DifferentialEquations.Jl – A Performant and Feature-Rich Ecosystem for Solving Differential Equations in Julia. *J. Open Res. Softw.* **2017**, *5*, 15.

(7) Powell, M. J. D. The BOBYQA Algorithm for Bound Constrained Optimization without Derivatives. *Cambridge Numer. Anal. Rep.* **2009**, NA2009/06.